2006-09

Steady state and transient measurements within a compressor rotor during steam-induced stall at transonic operational speeds

Zarro, Sarah E.

Monterey, California. Naval Postgraduate School

NAVAL POSTGRADUATE SCHOOL

MONTEREY, CALIFORNIA

THESIS

STEADY-STATE AND TRANSIENT MEASUREMENTS WITHIN A COMPRESSOR ROTOR DURING STEAM-INDUCED STALL AT TRANSONIC OPERATIONAL SPEEDS

by

Sarah E. Zarro

September 2006

Thesis Advisor:	Garth Hobson
Second Reader:	Reader's Name

Approved for public release; distribution is unlimited

THIS PAGE INTENTIONALLY LEFT BLANK

REPORT DOCUMENTATION PAGE		Form Approved OMB No. 0704-0188

1. AGENCY USE ONLY *(Leave blank)*	2. REPORT DATE September 2006	3. REPORT TYPE AND DATES COVERED Master's Thesis

4. TITLE AND SUBTITLE Steady-State and Transient Measurements Within a Compressor Rotor During Steam-Induced Stall at Transonic Operational Speeds	5. FUNDING NUMBERS
6. AUTHOR(S) Sarah E. Zarro	
7. PERFORMING ORGANIZATION NAME(S) AND ADDRESS(ES) Naval Postgraduate School Monterey, CA 93943-5000	8. PERFORMING ORGANIZATION REPORT NUMBER
9. SPONSORING /MONITORING AGENCY NAME(S) AND ADDRESS(ES) N/A	10. SPONSORING/MONITORING AGENCY REPORT NUMBER

11. SUPPLEMENTARY NOTES The views expressed in this thesis are those of the author and do not reflect the official policy or position of the Department of Defense or the U.S. Government.

12a. DISTRIBUTION / AVAILABILITY STATEMENT Approved for public release; distribution is unlimited	12b. DISTRIBUTION CODE

13. ABSTRACT (maximum 200 words)

Steam leakage from an aircraft carrier catapult is sometimes ingested into the aircraft engines upon launch which may induce compressor stall. Investigation of this phenomenon is of particular interest to the Navy with its new F35C, the aircraft carrier variant of the joint strike fighter. The single engine configuration of the F-35C makes this aircraft particularly vulnerable to steam-induced stall. The present study examined both throttle-induced stall and steam-induced stall in a compressor at 90% and 95% speed through the use of 9 Kulite and 2 hot-film pressure transducers. The use of Fast Fourier Transform waterfall plots of the transient data before and during stall proved invaluable in determining stall precursors as well as the mode of rotor stall.

In addition, a new computational fluid dynamic model was designed using CFX-5 software to represent a single blade passage of the compressor rotor, in order to predict compressor performance. The computed results were compared to experimental results gathered at various throttle settings. An accurate model will enable researchers to predict compressor performance for various and multiple gases.

14. SUBJECT TERMS Compressor, Transonic, Steam Ingestion, Turbulence, Stall, CFD, Computational Model	15. NUMBER OF PAGES 85
	16. PRICE CODE

17. SECURITY CLASSIFICATION OF REPORT	18. SECURITY CLASSIFICATION OF THIS PAGE	19. SECURITY CLASSIFICATION OF ABSTRACT	20. LIMITATION OF ABSTRACT
Unclassified	Unclassified	Unclassified	UL

NSN 7540-01-280-5500

Standard Form 298 (Rev. 2-89)
Prescribed by ANSI Std. 239-18

THIS PAGE INTENTIONALLY LEFT BLANK

Approved for public release; distribution is unlimited

STEADY-STATE AND TRANSIENT MEASUREMENTS WITHIN A COMPRESSOR ROTOR DURING STEAM-INDUCED STALL AT TRANSONIC OPERATIONAL SPEEDS

Sarah E. Zarro
Lieutenant, United States Navy Reserve
B.S., United Stated Naval Academy, 1999

Submitted in partial fulfillment of the
requirements for the degree of

MASTER OF SCIENCE IN MECHANICAL ENGINEERING

from the

NAVAL POSTGRADUATE SCHOOL
September 2006

Author: Sarah E. Zarro

Approved by: Prof. Garth V. Hobson
Thesis Advisor

Prof. Raymond P. Shreeve
Second Reader

Prof. Anthony J. Healy
Chairman, Department of Mechanical and Astronautical Engineering

THIS PAGE INTENTIONALLY LEFT BLANK

ABSTRACT

Steam leakage from an aircraft carrier catapult is sometimes ingested into the aircraft engines upon launch which may induce compressor stall. Investigation of this phenomenon is of particular interest to the Navy with its new F35C, the aircraft carrier variant of the joint strike fighter. The single engine configuration of the F-35C makes this aircraft particularly vulnerable to steam-induced stall. The present study examined both throttle-induced stall and steam-induced stall in a compressor at 90% and 95% speed through the use of 9 Kulite and 2 hot-film pressure transducers. The use of Fast Fourier Transform waterfall plots of the transient data before and during stall proved invaluable in determining stall precursors as well as the mode of rotor stall.

In addition, a new computational fluid dynamic model was designed using CFX-5 software to represent a single blade passage of the compressor rotor, in order to predict compressor performance. The computed results were compared to experimental results gathered at various throttle settings. An accurate model will enable researchers to predict compressor performance for various and multiple gases.

THIS PAGE INTENTIONALLY LEFT BLANK

TABLE OF CONTENTS

LIST OF FIGURES

LIST OF TABLES

THIS PAGE INTENTIONALLY LEFT BLANK

ACKNOWLEDGMENTS

I would first like to thank Professor Hobson, whose unfailing support and patience even when everything was going wrong made this thesis possible. I would also like to thank Professor Shreeve who ensured my work was honest, accurate, and brief. Anthony Gannon's technical knowledge and ability to make even the most unruly computer software work while maintaining his sense of humor was invaluable. Finally, I would like to thank Rick and John, the men behind the curtain, who truly make the equipment run, can weld or fabricate anything you could think of, and can make the best of the worst of times.

THIS PAGE INTENTIONALLY LEFT BLANK

I. INTRODUCTION

As the U.S. Navy transitions to the new F-35C Joint Strike Fighter (JSF), concern regarding the occurrence of steam-induced stall during catapult launches has increased. Research conducted at Naval Air Engineering Station Lakehurst with an F-18 has shown the susceptibility of jet engines to stall after ingesting steam. The F-35C, with a single engine, is clearly particularly vulnerable to catastrophic loss should the engine stall as a result of ingesting steam leaking from aging aircraft carrier catapults.

The research conducted at the Turbopropulsion Laboratory at the Naval Postgraduate School is presently focused on the effects of steam ingestion on a transonic compressor rotor. The complete rotor-stator transonic compressor fan stage was specifically designed for the Naval Postgraduate School by Sanger at the NASA Glenn Research Center (Refs. 1 and 2), to be evaluated in the Transonic Compressor Rig (TCR).

The performance characteristics of the compressor in both the fan-stage as well as the rotor-only configurations were mapped by Gannon, Hobson and Shreeve. Utilizing this data, the performance characteristics at 70%, 80%, 90% and 100% speed prior to and during stall were established (Refs. 3-5). Rodgers reestablished unsteady pressure measurements at 60%, 70%, and 80% speed (Ref. 6). Inlet and exit surveys at 70%, 80%, 90% and 100% speed were conducted with a three-hole probe by Villescas, who then determined the spanwise diffusion-factor distribution of the rotor at choke, peak efficiency, and stall (Ref. 7). Brunner repeated the inlet surveys with a 5-hole probe and determined the pitch angle and Mach number distributions for the rotor inlet (Ref. 8). Payne, using both hot-film and Kulite pressure transducers, mapped 95% design speed to near stall and 70% design speed to steam-induced stall (Ref. 9). Levis increased the number of Kulite pressure transducers to nine, mapped 90% design speed up to steam-induced stall, and re-established the 70% design speed stall and steam stall points after the replacement of the inlet honeycomb flow straightener (Ref. 10).

The current study completed the feasible performance mapping of the rotor-only configuration to 95% of design speed. By replacing the previous pneumatic Scanivalve

system with three Model 3217 Digital Sensor Arrays (DSA) and rewriting the HP-VEE performance program to interact with them, pressure readings were made more efficiently, which resulted in less wear and tear on the TCR. Nine Kulite pressure transducers in the case wall, one impact Kulite probe, and two hot-film transducers were utilized to measure rotor characteristics prior to and during steam-induced stall. The effect of steam ingestion upon the displacement of the stall line at 90% and 95% speed, during which time the rotor tip relative speeds were transonic, was measured.

A refined computational grid (Ref. 11) was generated of a single rotor passage for the numerical investigation of the steady-state performance of the rotor. Favorable comparisons with the experimental data at 90% and 95% speed were calculated.

II. EXPERIMENTAL FACILITY AND EQUIPMENT

A. TRANSONIC COMPRESSOR ROTOR

For the most recent studies, a rotor-only assembly was evaluated in order to simplify the configuration and minimize the potential damage in the event of a catastrophic failure during stall.

The Transonic Compressor Rig (TCR), as shown in Figure 1, was driven by two opposed-rotor air turbine stages, supplied by a 12 stage Allis-Chalmers axial compressor. The rotor had 22 blades and was made from a high strength aluminum alloy (7075-T6). The design specifications for the Sanger Stage are given in Table 1. Air was drawn into the TCR from the atmosphere through a throttle valve and a honeycomb flow straightener. The air passed down a five-meter long 46 cm diameter pipe connecting the settling chamber to the test compressor. The air passed through a nozzle, used to measure the mass flow rate, and was exhausted back to the atmosphere aft of the test compressor.

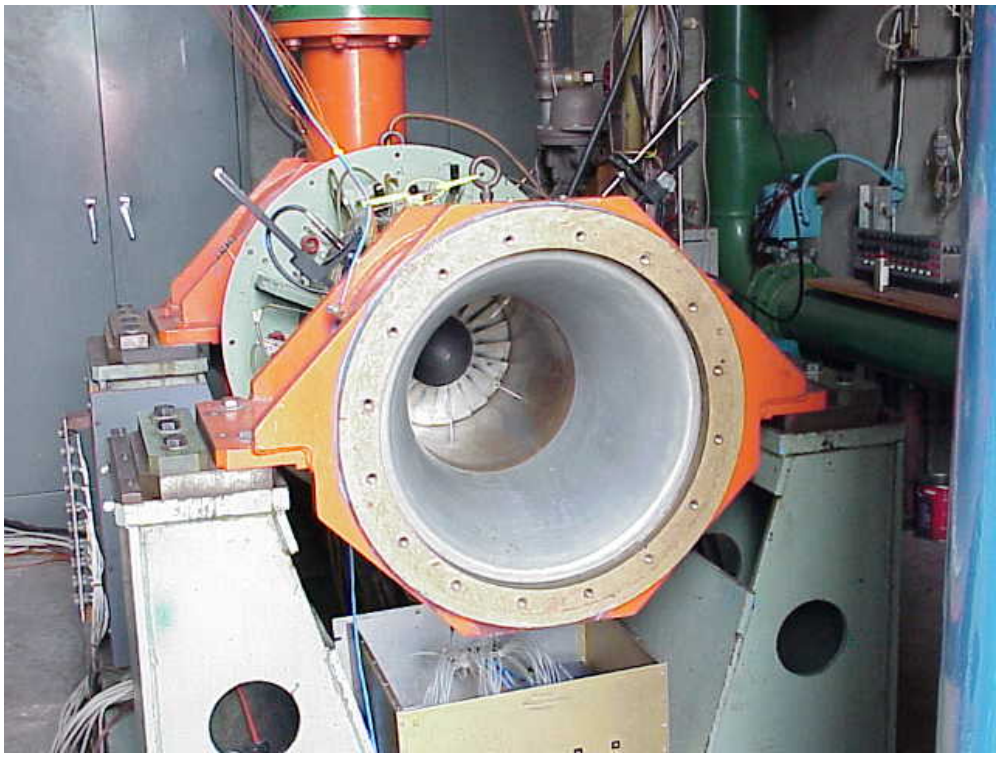

Figure 1. Transonic Compressor Rig, with Inlet Piping Removed

Table 1. Sanger Stage Parameters

Parameter	Value
Pressure Ratio	1.61
Tip Speed	33.02 m/s (1300ft/s)
Design Speed	27085 rpm
Design Mass Flow	7.75 kg/s (17.05lb/s)
Specific Mass Flow	170.88 kg/s-m^2 (35lbm/s-ft^2)
Specific Head Rise	.246
Tip Inlet Relative Mach Number	1.28
Aspect Ratio	1.2
Hub/Tip Radius Ratio	.51
Rotor Inlet Ramp Angle	28.2
Number of Rotor Blades	22
Tip Solidity (Rotor)	1.3
Outside Diameter	0.2794m (11 inches)
Rotor Diffusion Factor – Tip	.4
Rotor Diffusion Factor - Hub	.47

B. STEAM INGESTION SYSTEM

In order to generate the required pressure of steam for this experiment, a Sussman model SVS600 steam boiler, capable of producing saturated steam up to a pressure of 1000 kPa or 1.4 kg/sec at 100 ˚C, was utilized (Ref. 12). The transient response of the steam pressure was monitored through the use of a pressure transducer installed in the steam pipe (Figure 2). Two remotely-operated, fast-acting solenoid valves were used to release the steam into the intake plenum as well as to initially vent the pipe to preheat and prevent condensation. Consistency in temperature readings from the inlet thermocouple after it was moved from the 6 o'clock (Refs. 9 and 10) to the 8 o'clock position confirmed that, after ingestion of steam, the entire compressor inlet saw a consistent

mixture of steam and air. The compressor rig and steam ingestion system are shown schematically in Figure 2 and a photo of the intake plenum, TCR, inlet piping, and steam generator are shown in Figure 3.

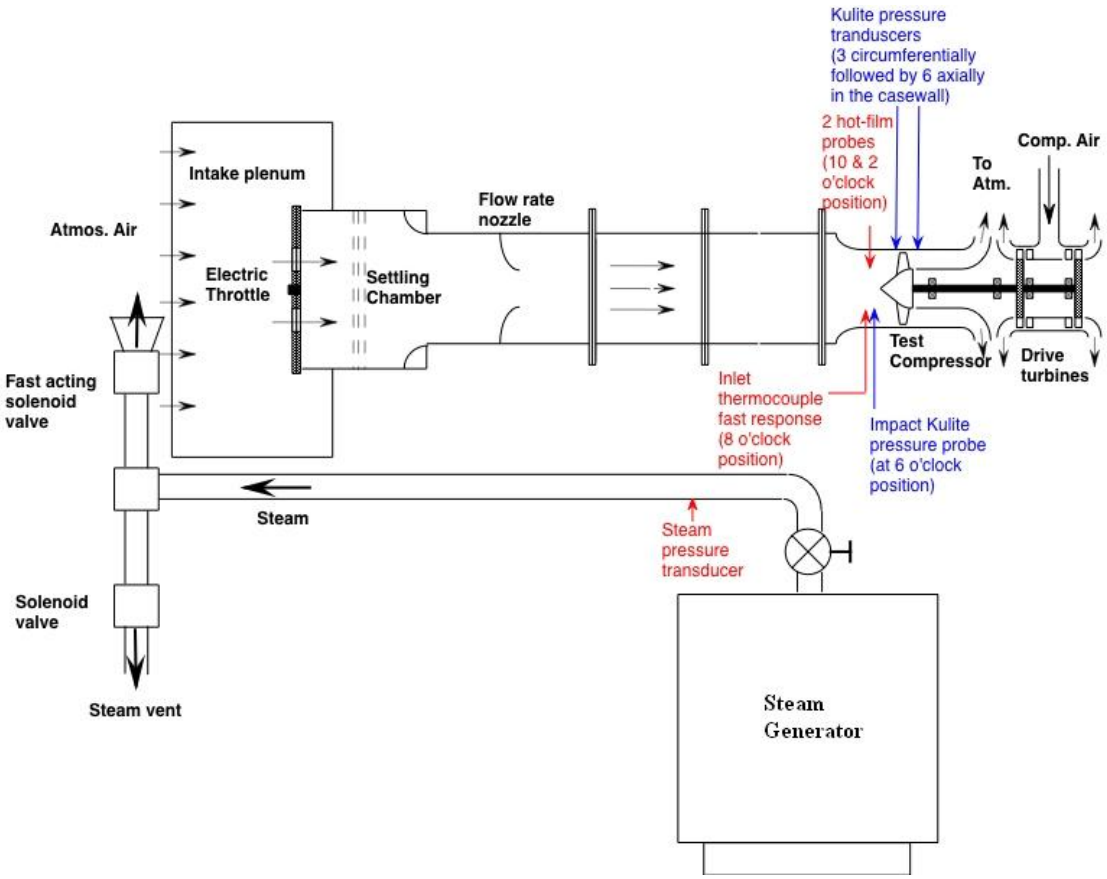

Figure 2. Transonic Compressor Rig with Steam Ingestion System

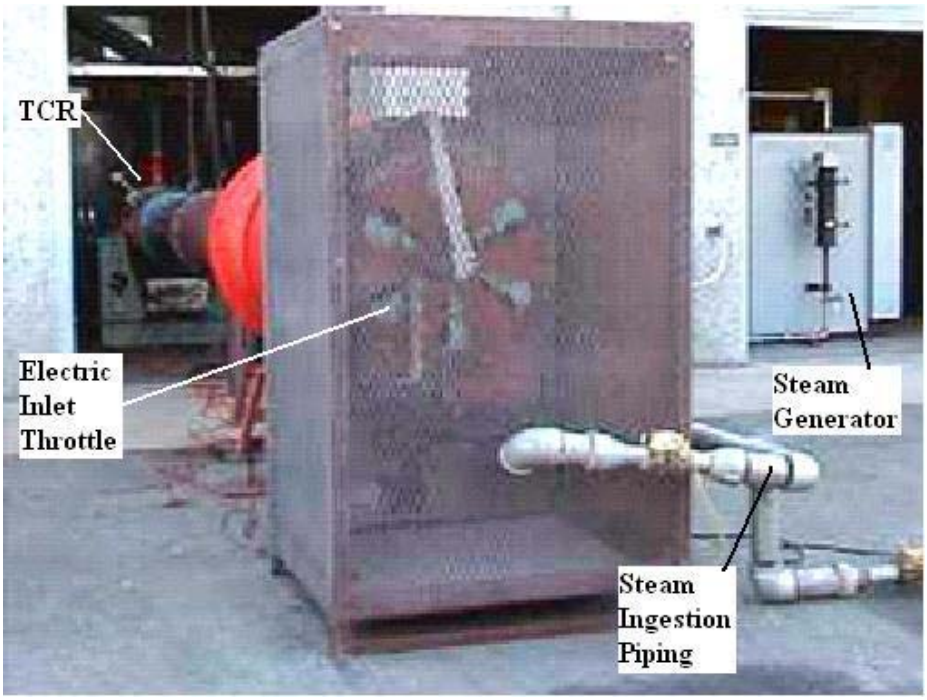

Figure 3. Intake Plenum and Steam Ingestion System

III. INSTRUMENTATION

A. PROBES

1. Hot-Film

Inlet-flow conditions were characterized using hot-film anemometry measurements. Measurements were taken using two 20 micron TSI model 1212-20 hot-film probes (Figure 4, Ref. 12) with serial numbers 70618113 and 70618114. Data were acquired using an IFA 100 Intelligent Flow Analyzer, and TSI ThermalPro software version 4.53, running on a PC.

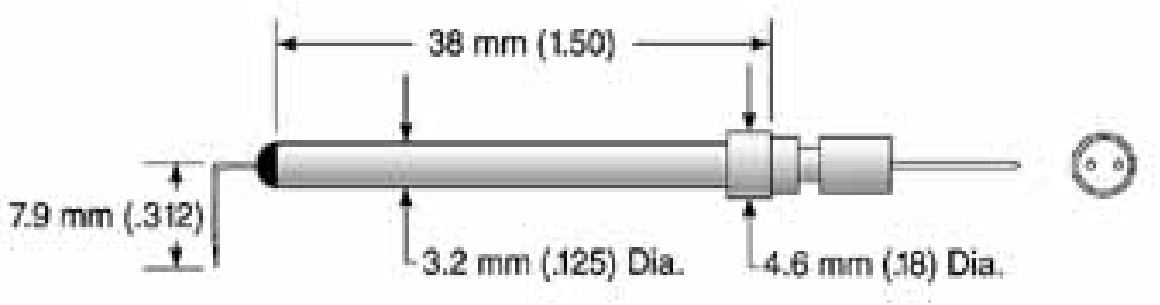

Figure 4. TSI Model 1212-20 Hot-Film Probe (From Ref. 12)

2. Kulite Pressure Transducer

A model XCQ-080-25 Kulite miniature silicon pressure transducer was used to obtain time-resolved pressure data. The probe was a miniature, semiconductor, strain-gauge transducer which incorporated a fully active four-arm Wheatstone bridge dielectrically isolated silicon-on-silicon diaphragm. A diagram of the probe is given in Figure 5 and the specifications are given in Table 2.

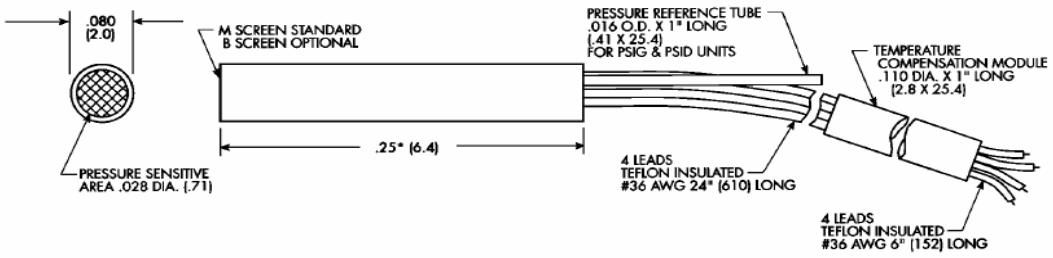

Figure 5. Kulite XCQ-080 Series Transducer (From Ref. 6)

Table 2. XCQ-080-25 Factory Specifications (From Ref. 5)

Input	
Pressure Range	25 psi
Over Pressure	50 psi
Burst	75 psi
Rated Electrical Excitation	10 VDC/AC
Maximum Electrical Excitation	15 VDC/AC
Input Impedance	800 Ohms
Output	
Output Impedance	1000 Ohms
Full Scale Output	100 mV
Residual Unbalance	+-3 % FSO
Non-Linearity and Hysterisis	0.1 % FS BFSL
Hysteresis	0.1 %
Repeatability	0.1 %
Resolution	Infinite
Natural Frequency	300 kHz
Perpendicular Accel Sensitivity	0.0003 % FS/g
Transverse Accel Sensitivity	0.00004 % FS/g
Insulation Resistance	100 Megohm
Environmental	
Operating Temp Range	-65 to 250 deg F
Compensated Temp Range	80 to 180 deg F
Thermal Zero Shift	+- 1 % FS/100 F
Thermal Sensitivity Shift	+- 1 % FS/100 F

3. Fine-Wire Thermocouple

An OMEGA fine-gage thermocouple was used to obtain fast, accurate temperature measurements of the steam in the inlet to the TCR. The thermocouple utilized J-Type wires of diameter 0.025 mm and was capable of obtaining accurate temperature measurements in both air and water. A diagram of the thermocouple is given in Figure 6 and the specifications are given in Table 3.

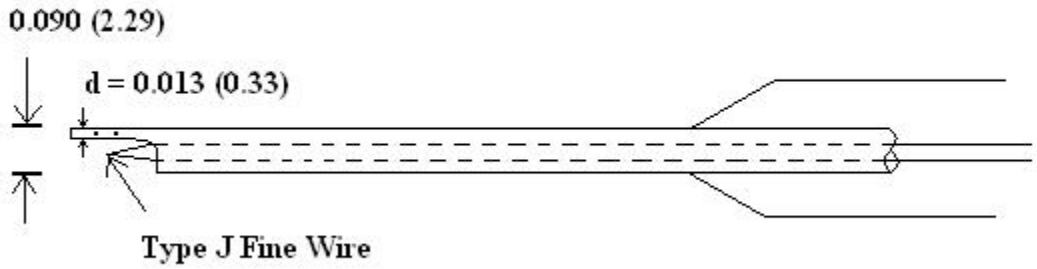

Figure 6. Fine Gage Microtemp Thermocouple

Table 3. Thermocouple Response Time

Wire Size mm (inches)	Still Air 427C/38C 800F/100F	60 ft/sec Air 427C/38C 800F/100F	Still H2O 93C/38C 200F/100F
0.025 (0.001)	0.05 sec	0.004 sec	0.002 sec

B. INSTALLATION OF SENSORS

1. Hot-Film

Two hot-film probes were installed, as shown in Figure 7, through the case wall 11.5cm upstream of the leading edge of the rotor, and extended 4cm into the flow. The sensors were positioned at the 2 and 10 o'clock positions and faced toward the inlet flow. Adding a second probe allowed for redundancy, in case of failure, and for comparison of results.

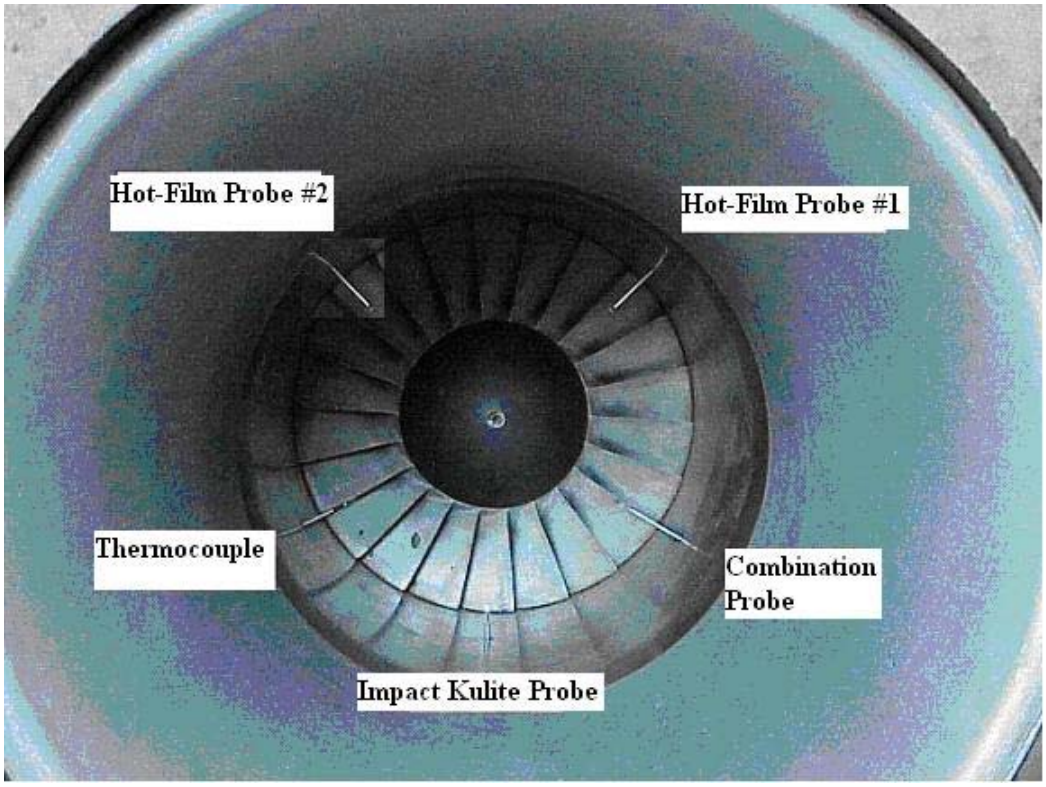

Figure 7. Probe Location in TCR Inlet

2. Kulite Pressure Transducer

Nine Kulite pressure transducers were placed in the case wall at various locations axially and peripherally to examine the effect of stall on the case wall pressure, as shown in Figures 8 and 9.

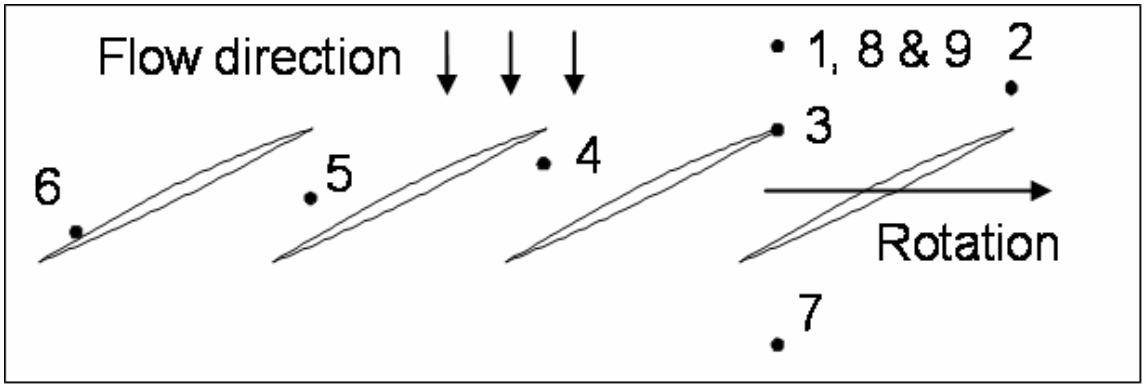

Figure 8. Kulite Position Relative to Rotor Blades

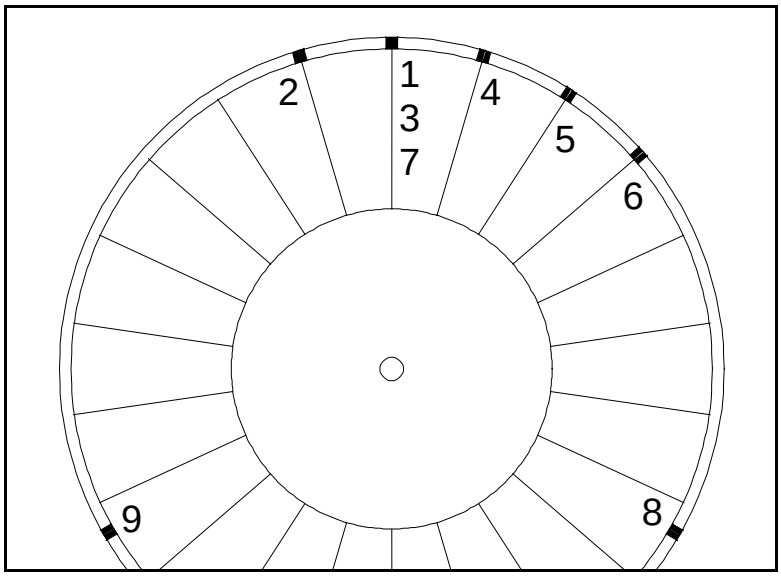

Figure 9. Kulite Position in Case Wall

One impact Kulite probe was installed at the 6 o'clock position. The probe was directed upstream and had a vertical row of holes drilled on its face instead of the standard screen which is shown in Figure 5.

C. DATA ACQUISITION

1. Hot-Film and Kulite Data Acquisition

Hot-film data were acquired as described by Payne (Ref. 9). Kulite Data were acquired as described in detail by Levis (Ref. 10). Figure 10 is the combined Kulite and hot-film data acquisition system.

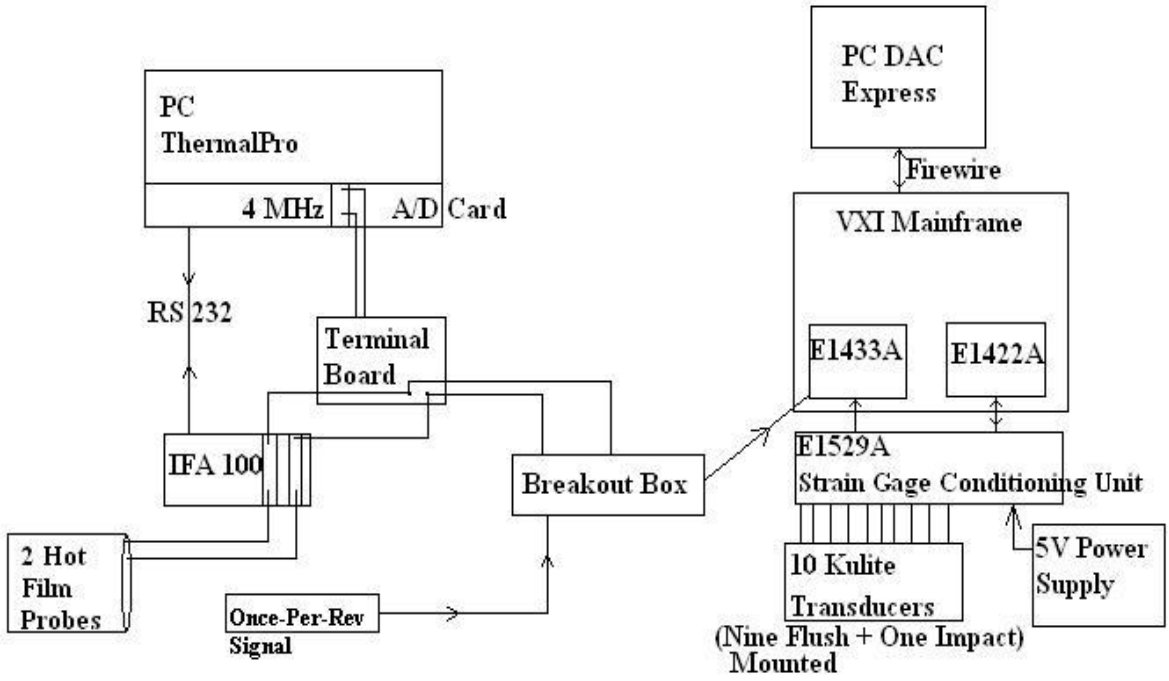

Figure 10. Transient Hot-Film and Kulite DAC Systems

2. Digital Sensor Array

The Digital Sensor Array is a stand-alone temperature compensated electronic pressure scanner capable of up to 16 individual or 8 differential pressure readings (Ref. 13). Each pressure sensor is calibrated to work within a temperature range of 0 to 59˚C. Each unit is assigned a specific IP Address enabling it to receive commands and return data via the Ethernet. The unit IP Address had to be renamed in order to make it compatible with the laboratory local area network (LAN) (see Appendix A).

Data were transferred directly from the DSA 3217 pressure bricks to an EXCEL spreadsheet via the Ethernet connection and the HPVEE computer program TCR.vee, which converted the binary data to engineering units (Pa) (Refs. 13 and 14). Pressure readings could also be acquired individually from the bricks using the DSALink 3 program, Figure 11, by pressing the start button (traffic sign) and the stop button (stop sign).

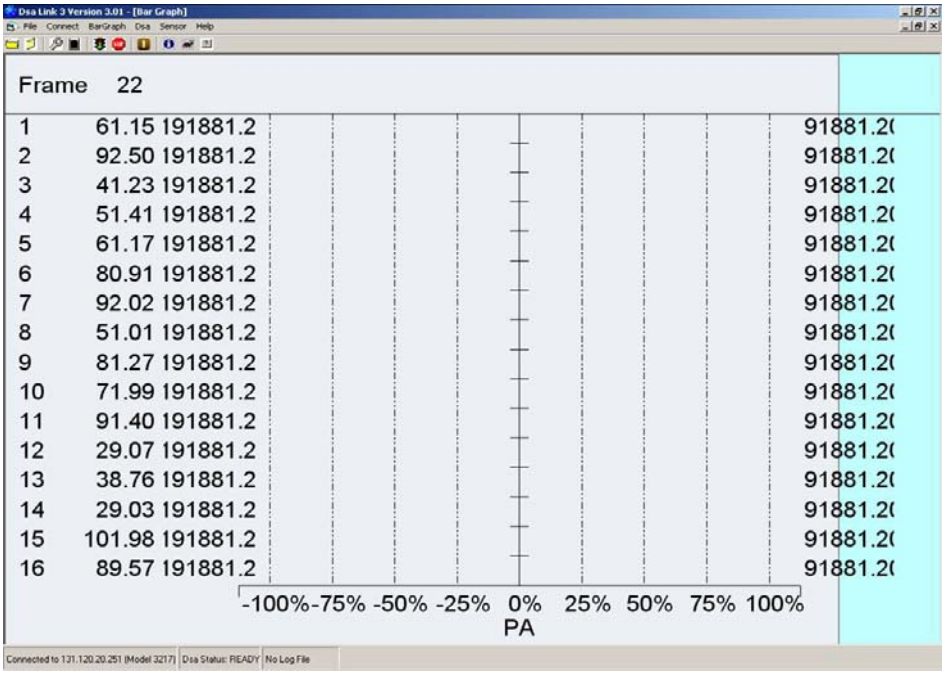

Figure 11. DSALink 3 Front Panel to Acquire Data from a DSA.

THIS PAGE INTENTIONALLY LEFT BLANK

IV. EXPERIMENTAL PROCEDURE

A. HOT-FILM CALIBRATION

The hot-film probes were individually calibrated after being positioned inside the compressor inlet, using the calibration procedure detailed in Appendix B. First a shorting probe was inserted and the cable resistance recorded with the IFA 100. The shorting probe was removed, replaced by a hot-film probe, and the new resistance read. The IFA 100 was adjusted for the probe's operating resistance and the appropriate bridge compensation. The compressor was started and its speed increased to 30% of maximum speed. Once speed stabilized, the differential pressure, the difference between static and stagnation pressure, was calculated and entered into the ThermalPro calibration software, and a calibration point was recorded. This step was repeated in increasing increments of 10% to 100% speed. The software applied curve fitting and calculated King's Law coefficients which were recorded and saved for future data analysis. During this process, a constant density was assumed which led to a maximum possible error of 12%.

B. DIGITAL SENSOR ARRAY SETUP AND OPERATION

The DSA units were factory calibrated, so no calibration was required. The units were energized and at least 30 minutes was allowed for warm up prior to use. The DSALink 3 software was used to connect to each unit to check its status and conduct a zero calibration prior to pressures being applied. The ScanPressures.vee program was run to complete DSA setup, changing its data output to binary and pressure readings to Pascals. The TCR.vee program (Figure 12) was used during compressor operation to measure steady-state pressures and temperatures throughout the TCR and calculate the performance of the compressor rotor.

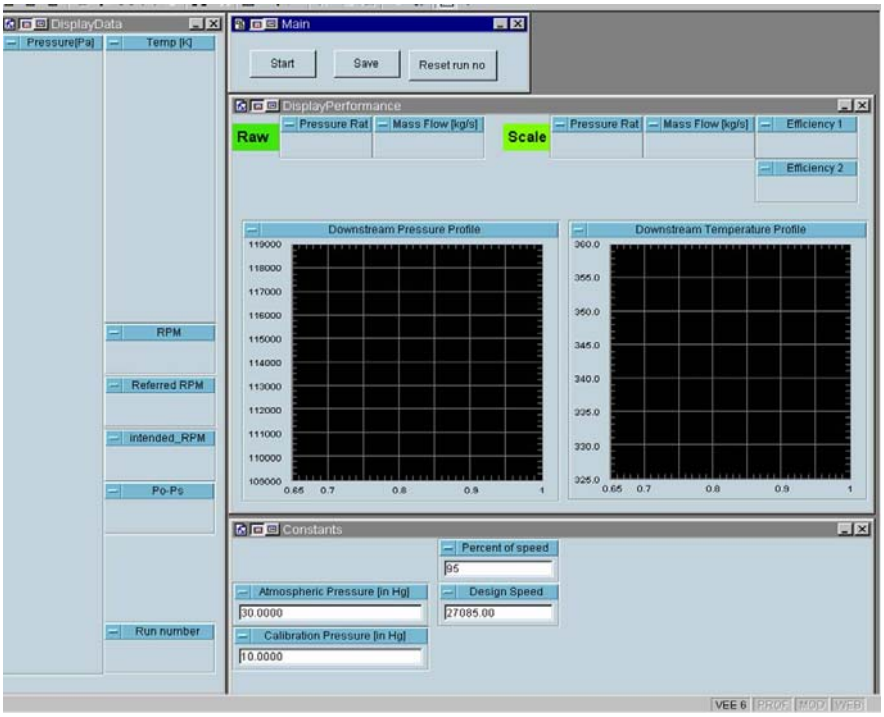

Figure 12. TCR.Vee Program

C. COMPRESSOR OPERATION

The standard procedure for operating the TCR was to increase to the appropriate speed with the throttle fully open. While maintaining constant rotor speed, the compressor throttle position was changed so measurements could be taken at different mass flow rates. By measuring mass flow rate, inlet and exit total temperatures and pressures the total-to-total pressure ratio and isentropic efficiency were calculated and the compressor performance was mapped for various speeds from open throttle to throttle-induced stall. Measurement and calibration procedures were described in more detail by Gannon et al. (Ref. 3). Normal speeds used are shown in Table 4.

Table 4. TCR Speed Settings

Percent Speed	RPM
100	27085
95	25730
90	24376.5
70	18959.5

D. HOT-FILM MEASUREMENTS

Data were taken at 90 and 95% speed in order to calculate the compressor inlet average velocity and turbulence intensity. Hot-film measurements were also used to study the airflow prior to and during stall to investigate possible precursors to stall. Measurements were taken at open throttle, peak efficiency, near stall, throttle-induced stall, and steam-induced stall. The steps in using the IFA 100 to collect data for two hot-film probes are detailed in Appendix C. The ThermalPro software was set to read both probes at a rate of 100,000 Hertz. For open throttle, peak efficiency, and near stall, the sample size was set to 8 kpts/ch, which lasted 0.0819 seconds. The sample size was increased to 512 kpts/ch for the stall runs to ensure that both the precursor and stall event were captured in a single file which lasted 5.2429 seconds.

E. STALL RUNS

In order to initiate a throttle-induced stall, the compressor speed was increased to 90 or 95% speed. The inlet throttle was closed incrementally, with readings taken at each setting, until compressor stall occurred. For both speeds, stall occurred as the throttle was closed from the 7.2 position (72% closed).

For steam-induced stall, the compressor was throttled to near stall conditions, at which time steady-state measurements were taken. The boiler isolation valve and steam vent solenoid valve were both opened to heat the steam piping in order to prevent condensation. After the piping was fully heated, the vent valve was closed and the data trace from the pressure transducer and thermocouple was started, (Figure 13). When the pressure in the pipe reached a target pressure, the isolation valve was closed. A countdown to steam release commenced, at which time the Kulite and hot-film data acquisition were initiated. At the end of the countdown, the main steam valve (fast-acting solenoid valve) was opened, allowing the steam to dump into the inlet plenum of the compressor. The suction at the inlet drew the steam down the piping and into the compressor. After several seconds, all data acquisition was stopped. The whole procedure was repeated at reduced throttle settings until stall occurred.

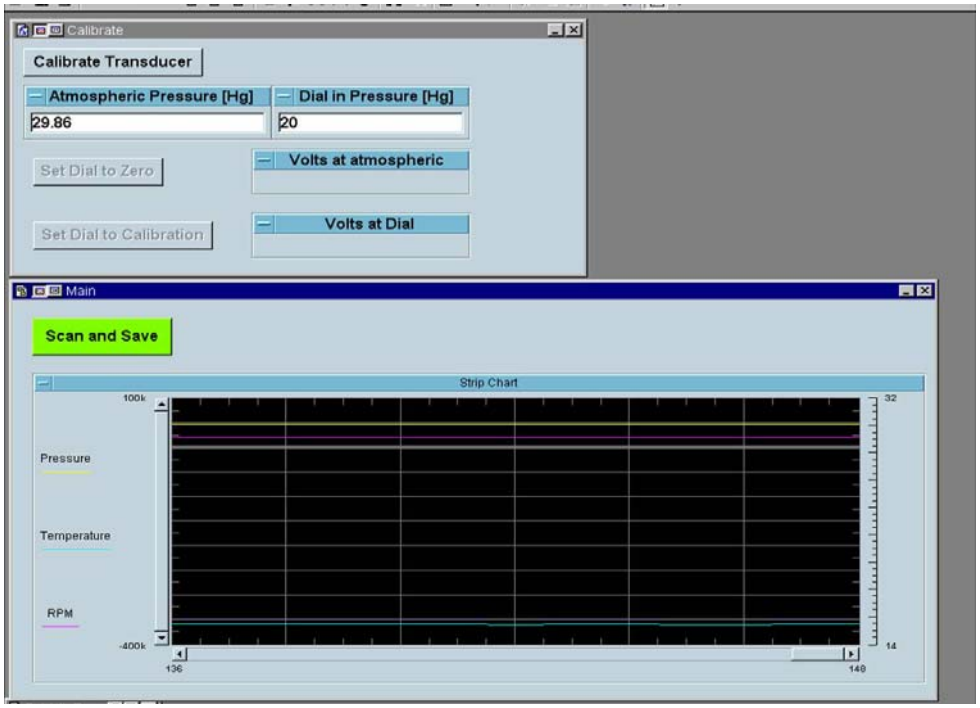

Figure 13. Strip Chart Program

V. PROCEDURE FOR COMPUTER SIMULATION

A. ICEM-CFD

ICEM-CFD was a CFX-5 compatible Computer Aided Design (CAD) program that allowed a user to create or import the geometry of their choice. In this case, the imported geometry (Ref. 15) was of a single blade and its passage from inlet to outlet of the compressor. A block was created to encompass the entire blade passage, its nodes made periodic (circumferential angle 16.3636˚), and its edges associated to the passage edges. An H-grid was created around the blade and its edges and vertices associated to those of the blade. Extra vertices were added to fit the H-grid to the curvature of the blade. After selecting the block representing the blade only, an O-grid was formed to enable the user to refine the mesh near the blade. The block representing the blade was then deleted in order to create a mesh for only space in which air could flow. After creating a mesh over the entire grid with a maximum element size of 0.125, the mesh was refined by increasing the number of nodes to garner greater data regarding the tips and surface of the blade than the inlet or outlet. Figures 14, 15, and 16 show different views of the final mesh created and Table 5 gives the final number of elements used to generate the grid.

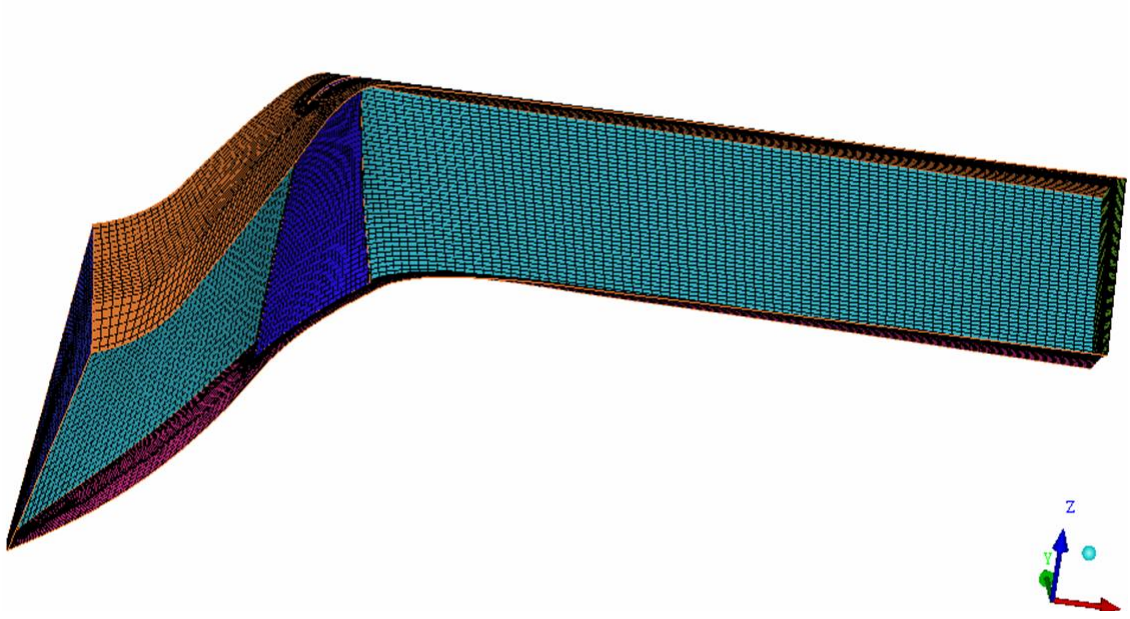

Figure 14. Blade Passage Mesh Created in ICEM-CFD

Figure 15. Hub Assembly Mesh Created in ICEM-CFD

Figure 16. Shroud Mesh Created in ICEM-CFD

Table 5. Number of Elements within the Mesh

Part	Elements
Blade	3280
Curves	1035
Exit	1000
Hub	4293
Inlet	1000
Passage 1	5560
Passage 2	5560
Points	14
Solid	171720
Tip	4293
Total Elements	197757
Total Nodes	184418

B. CFX-5

Previous studies capable of creating fairly accurate computational models of the rotor-only configuration were conducted with the SWIFT program using a very refined C-grid (Ref. 5). Unfortunately, the SWIFT program was not capable of incorporating a steam/air mixture. The new challenge has been to create a refined grid in the CFX-5 program which had a function to input a variety or mixture of gases and multiphase flows.

CFX-5 is comprised of three main functions: CFX-Pre, CFX-Solver, and CFX-Post. In CFX-Pre, the "turbo" mode was specified to ensure the program modeled turbomachinery flows. To most accurately model the real compressor, a k-ε turbulence model was used with the values of k and ε calculated from the experimentally calculated values of average velocity and turbulence intensity. Varied average exit static pressures were input as boundary conditions to model the throttling of the compressor. Figure 17 shows the model after all initial values were set. Further details regarding CFX-Pre setup may be found in Bochette (Ref. 11). CFX-Solver was set to conduct 1000 iterations in an attempt to converge the residual target to $1x10^{-6}$. If the solution was unable to converge in the first 1000 iterations, the CFX-Solver program allowed the user to continue solving from a previous file run. In CFX-Post, the results could be reviewed visually with the

turbo plotter which created color images of the blade passage and any variable the user desired. The program's function calculator was used to calculate the mass flow, mass-averaged pressure ratio, and temperature ratio to facilitate efficiency calculations.

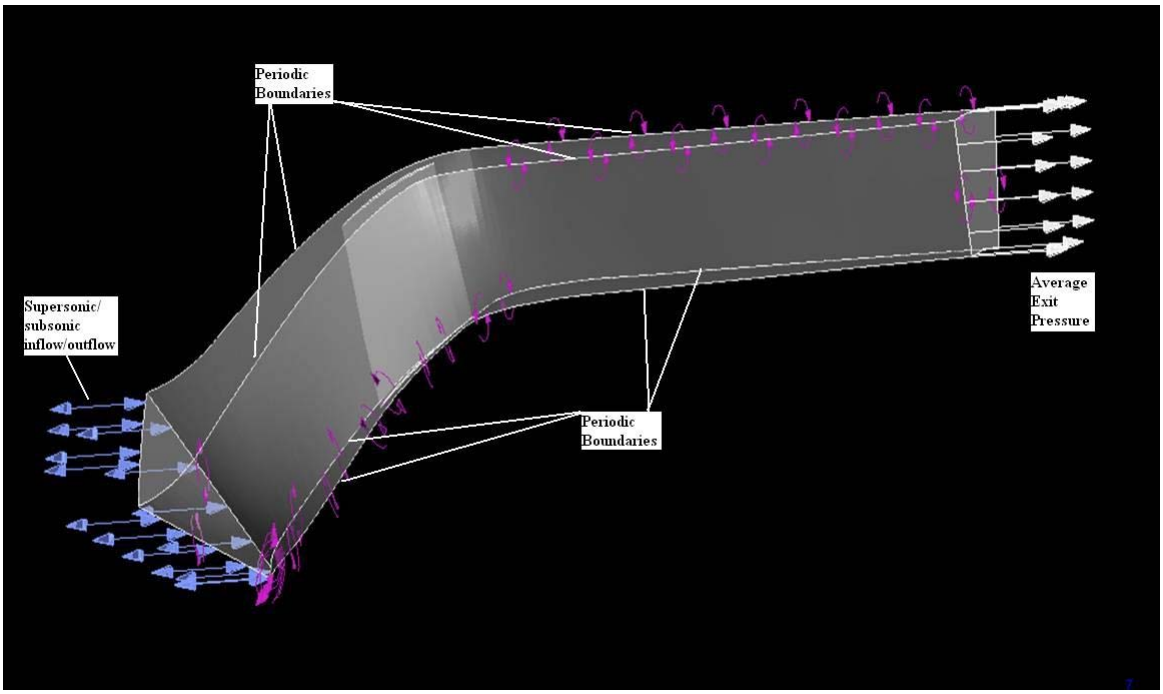

Figure 17. CFX-Pre Model of a Single Blade Passage of the TCR

VI. RESULTS AND DISCUSSION OF COMPRESSOR MAPPING

A. COMPRESSOR CHARACTERISTICS

Average velocity and turbulence intensity values were calculated using MATLAB code "hw.m" shown in Appendix D (Ref. 16). These values versus mass flow were then plotted in an EXCEL spreadsheet, as seen in Figures 18 through 21.

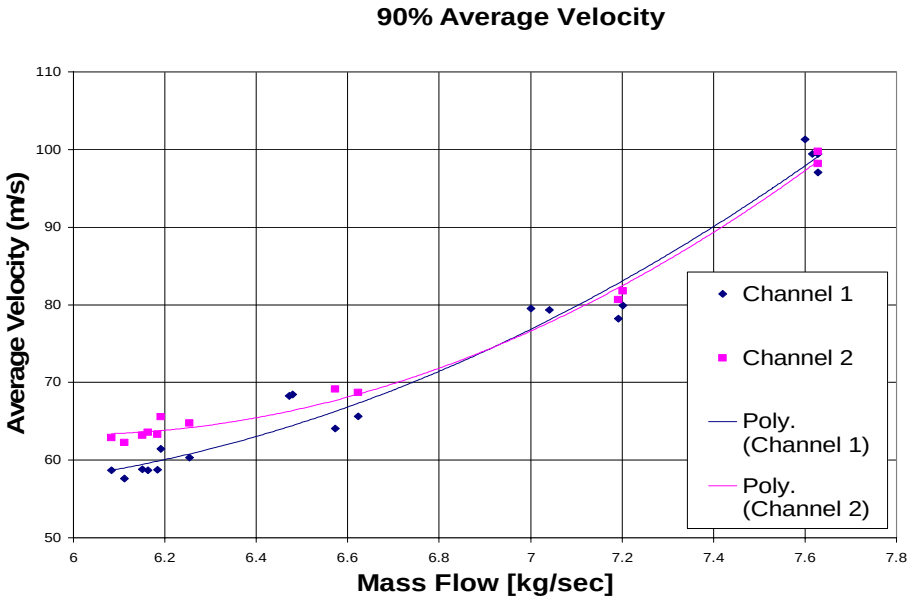

Figure 18. 90% Speed Average Velocity vs. Mass Flow Rate

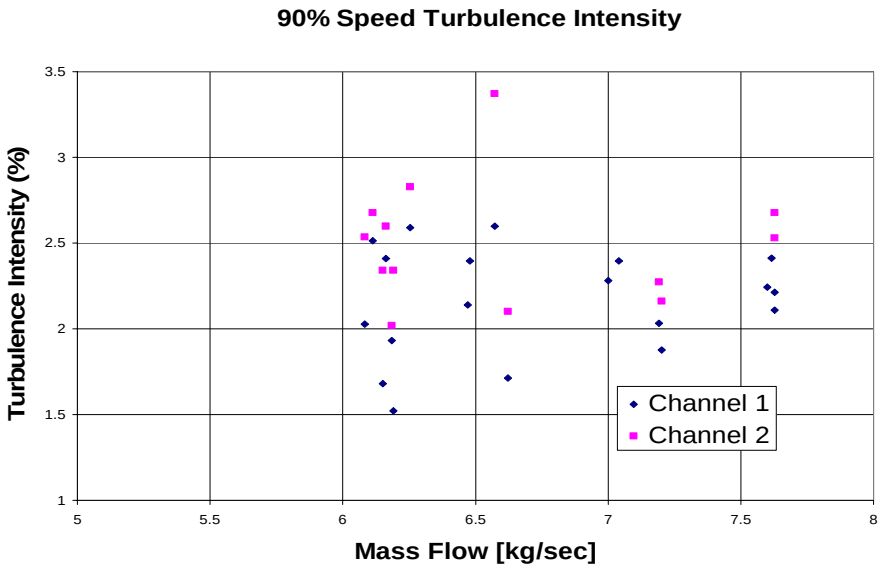

Figure 19. 90% Speed Turbulence Intensity vs. Mass Flow Rate

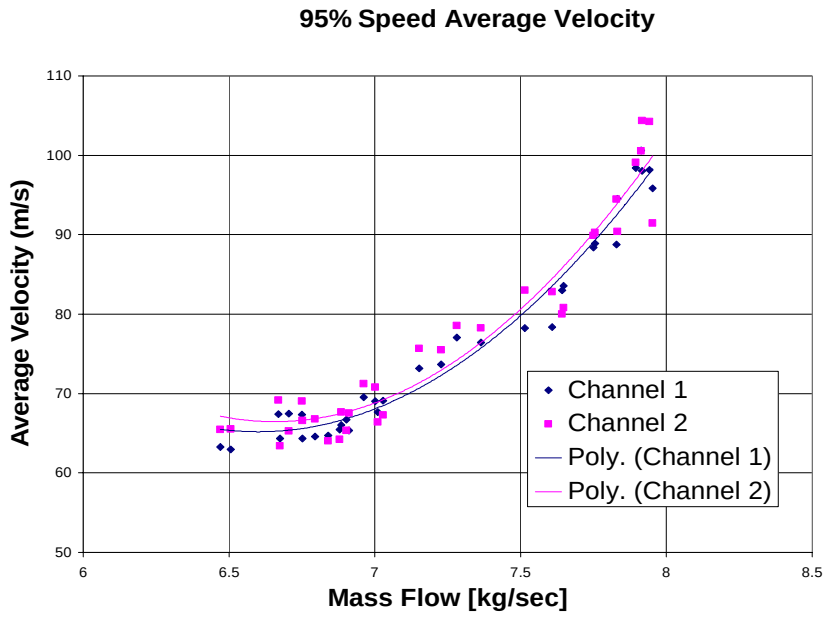

Figure 20. 95% Speed Average Velocity vs. Mass Flow Rate

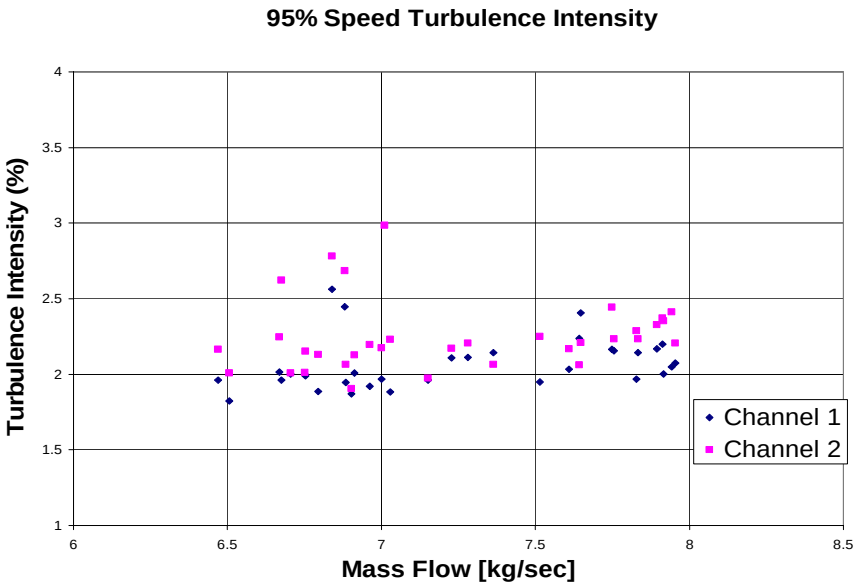

Figure 21. 95% Speed Turbulence Intensity vs. Mass Flow Rate

The average inlet velocity increased quadratically with throttle setting for both 90 and 95% speed. At 90% speed, the average turbulence intensity was 2.3%. At 95%, the average turbulence intensity was 2.2%. As may have been expected, this compressor characteristic appeared to be independent of compressor speed and throttle setting.

B. COMPRESSOR SPEED PERFORMANCE DATA

Continuing on compressor testing conducted by Gannon et al., Payne, and Levis (Refs. 3, 9, and 10 respectively), performance data from open throttle to stall were obtained. The results can be seen in Figures 22 and 23.

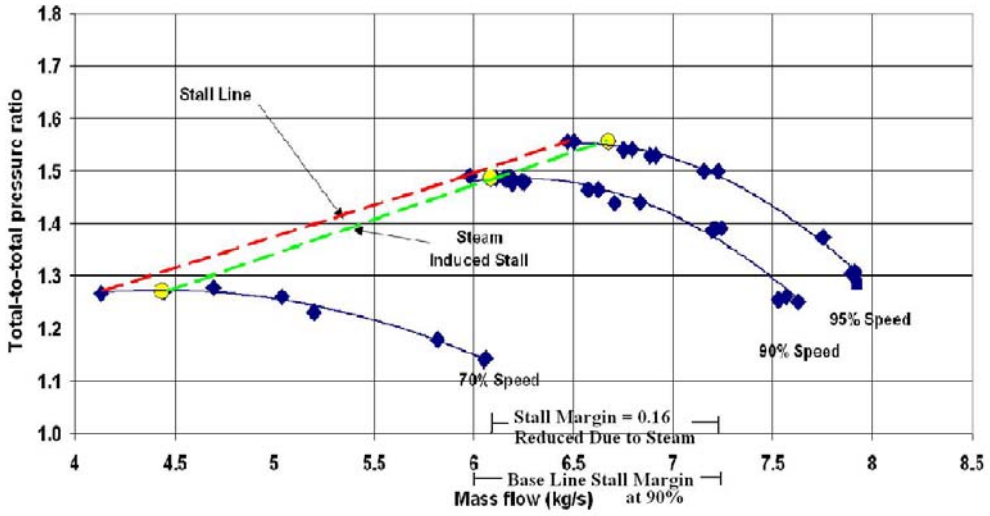

Figure 22. Compressor Pressure Ratio

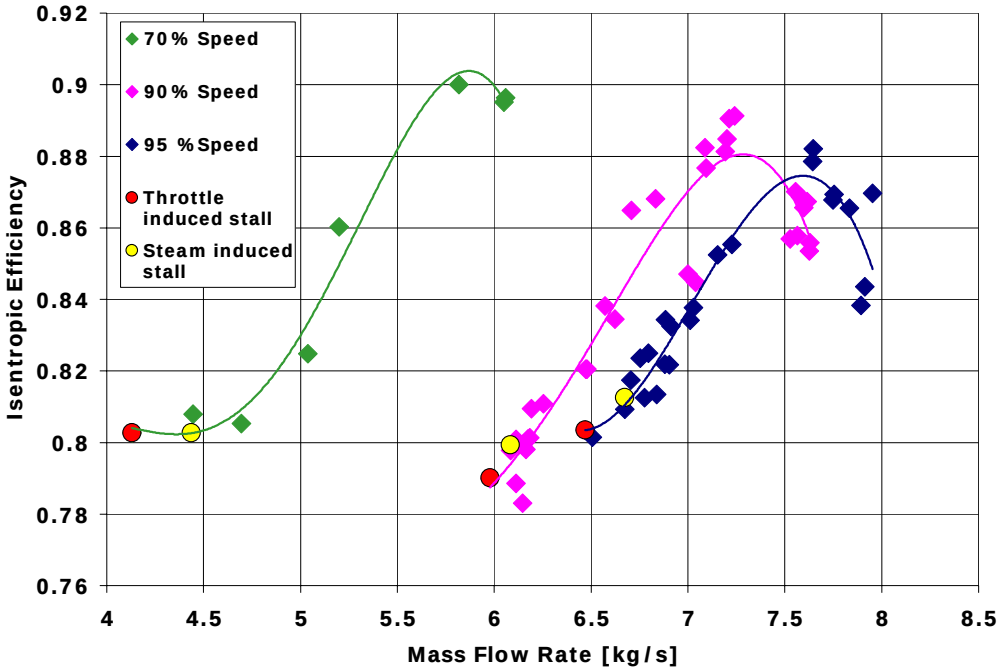

Figure 23. Compressor Efficiency (Fourth Order Polynomial Trendlines)

As can be seen, the stall line was displaced to the left due to steam ingestion of 0.12 kg/sec. For a particular speed line, the mass flow rate based stall margin is the mass flow rate at peak efficiency minus that at stall divided by the peak efficiency mass flow rate. At 90% speed, mass flow rate based stall margin was reduced from 0.17 to 0.16 due to a 2% steam mass flow rate. At 95% speed, mass flow rate based stall margin was reduced from 0.14 to 0.12.

Steam ingestion resulted in an increase in inlet temperature, which caused fluid density to decrease and the rotor to overspeed. This effect is displayed in Figures 24 and 25, which shows the drop in pressure in the steam line and the subsequent increase in inlet temperature due to steam ingestion during a stall event.

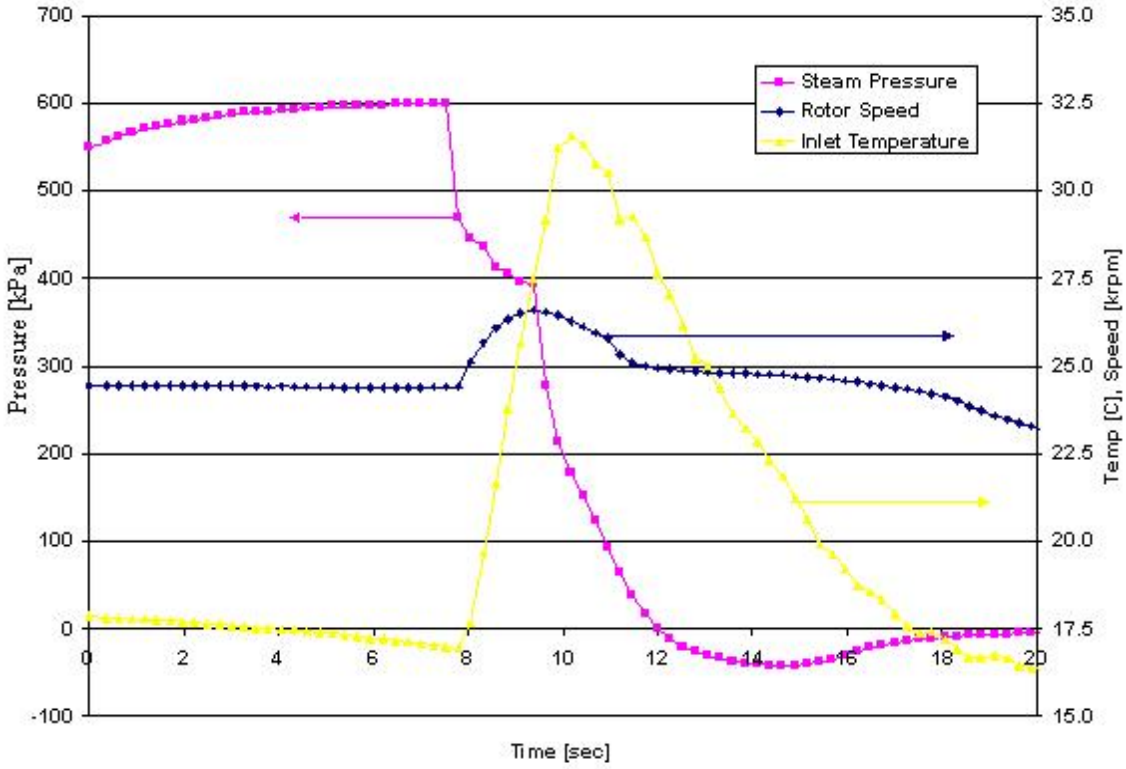

Figure 24. Steam Effects at 90% Speed

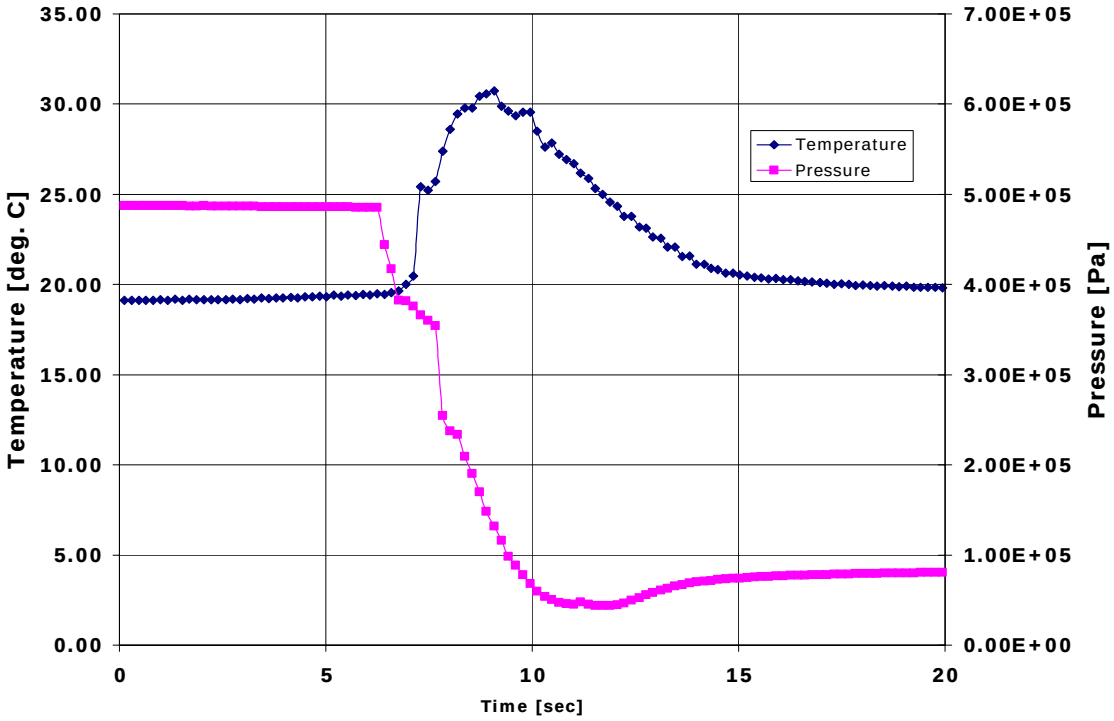

Figure 25. Steam Effects at 95% Speed

C. PEAK EFFICIENCY AND NEAR STALL STEADY STATE

Hot-film and Kulite measurements were made at peak efficiency and near stall. Contour plots and auto-correlation plots were developed from the measurements to develop a better understanding of the compressor characteristics and inlet flow behavior at different mass flow rates.

An auto-correlation plot was created with experimental hot-film data and MATLAB code fft_auto.m, Appendix D, and used to estimate the value of the integral time scale, Δt. The area under the curve is an indication of the length scale of the inlet turbulence. Figure 26 illustrates an example auto-correlation of data at 90% speed. Below is a sample calculation.

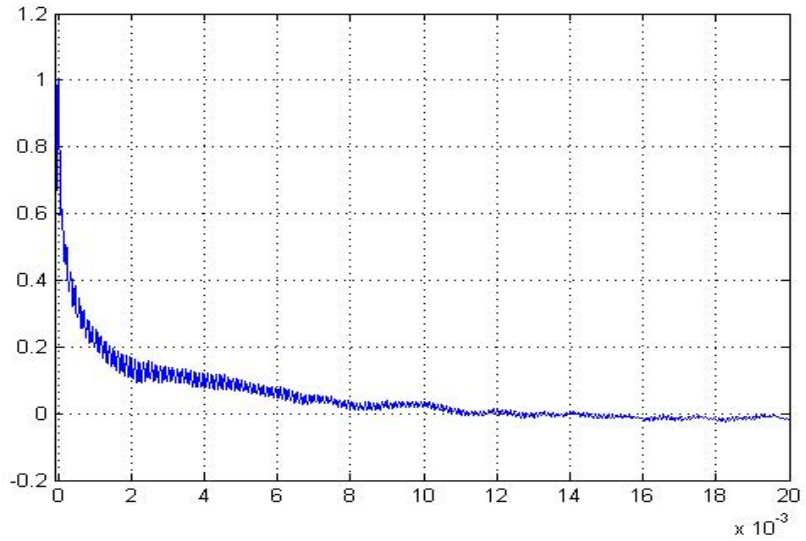

Figure 26. Auto-Correlation of Hot-Film Data at 90% Speed Near Stall

$\Delta t \approx 0.002$ (From above graph)

Ti = 0.020333 (Turbulence intensity from hw1.m)

$U_{avg} = 62.9$ (Average velocity from hw1.m)

$u'^2 = (Ti * U_{avg})^2 = 1.6357$

$k = 1.5*(u'^2) = 2.45355$

$L = \Delta t * U_{avg} = 0.1258$ (Turbulence length)

$\varepsilon = (C^{0.75} * k^{1.5})/(\kappa * L) = 12.55$ ($C = 0.09$, $\kappa = 0.4$)

Contour waterfall plots were created for Kulite #1, the impact Kulite and hotwire #1 for the cases of peak efficiency and near stall at 90% speed, Figures 27 through 32. The process was repeated for 95% speed, Appendix E.

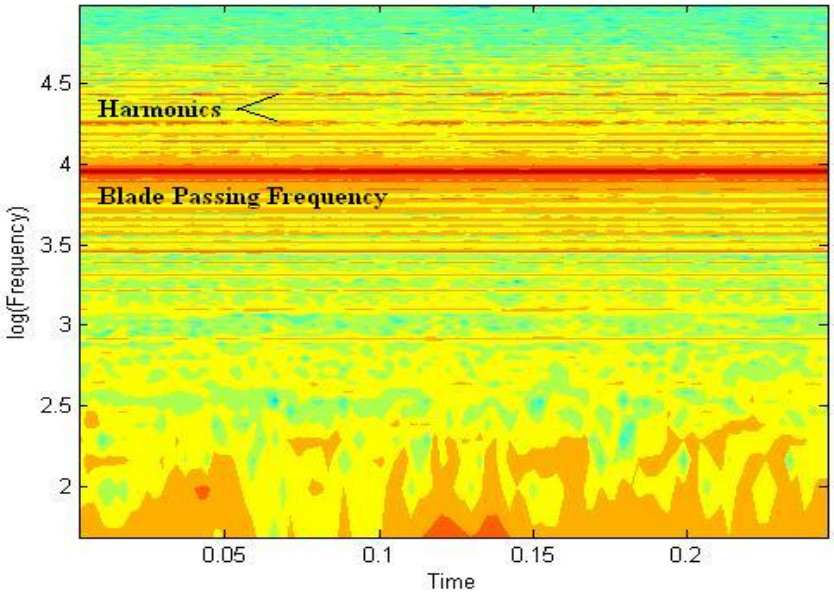

Figure 27. Kulite 1 at 90% Speed Peak Efficiency

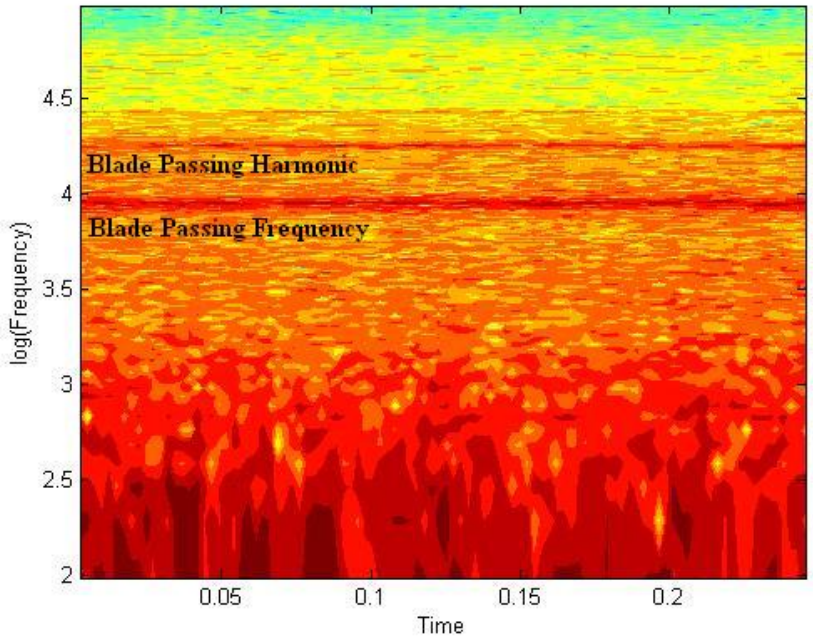

Figure 28. Impact Kulite at 90% Speed Peak Efficiency

The hot-film probes did not detect the once-per-rev signal because they were too far upstream of the rotor, however they did respond to the precursor signal which was a flow phenomenon. The Kulites being over the rotor did detect a once-per-rev signal.

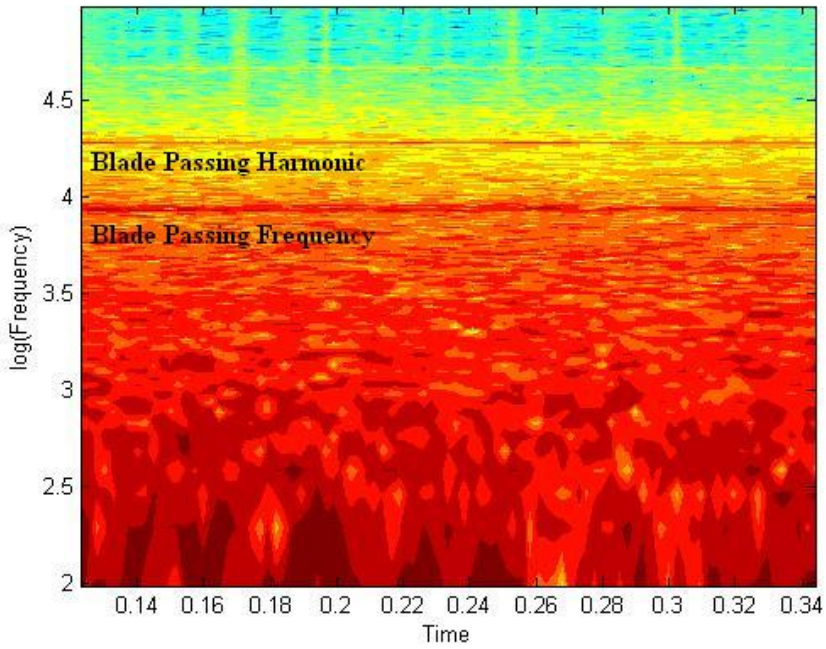

Figure 29. Hot-Film 1 at 90% Speed Peak Efficiency

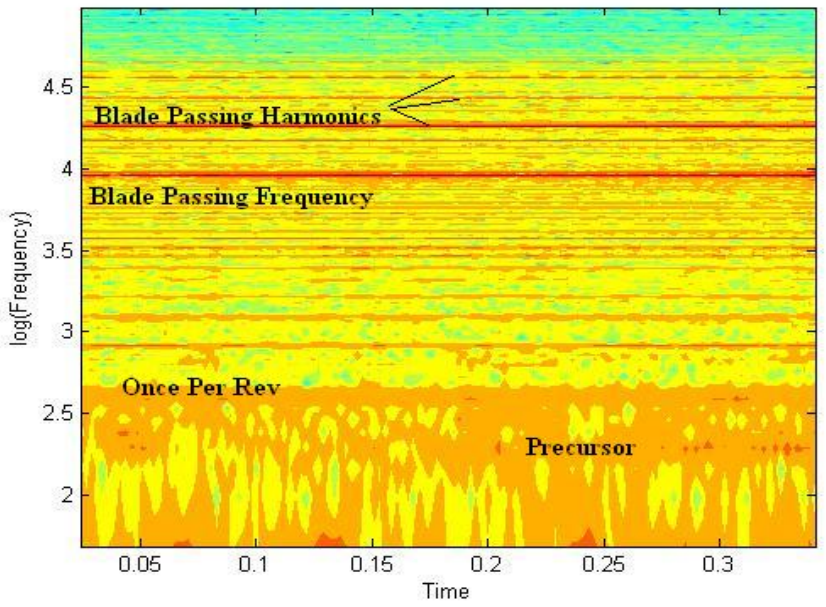

Figure 30. Kulite 1 at 90% Speed Near Stall

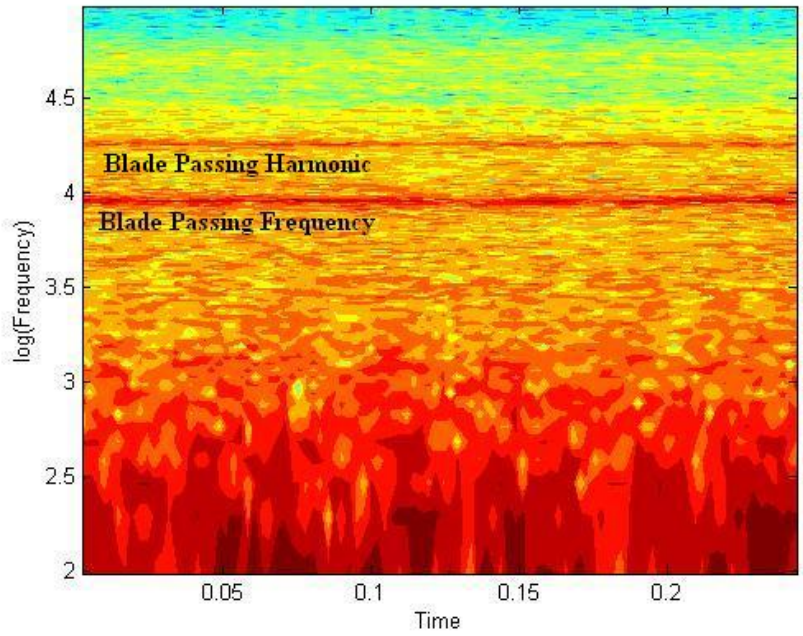

Figure 31. Impact Kulite at 90% Speed Near Stall

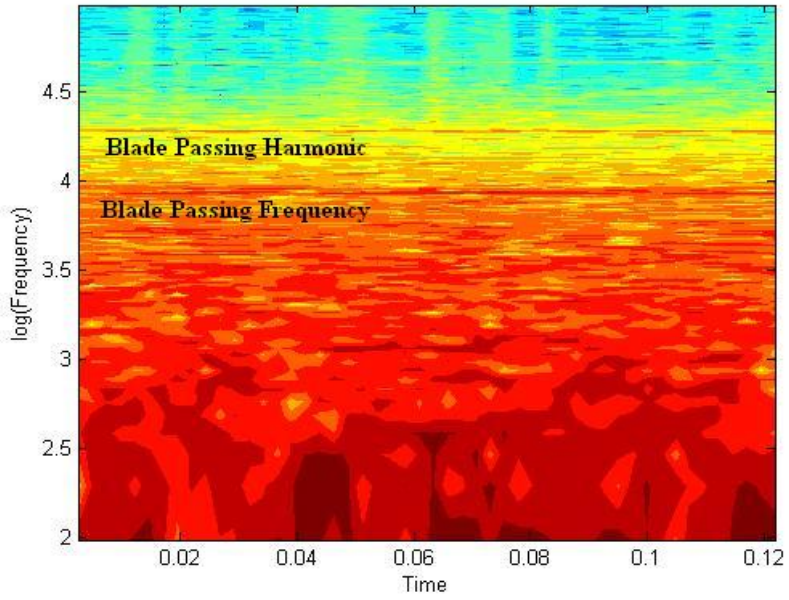

Figure 32. Hot-Film 1 at 90% Speed Near Stall

A stall precursor was only evident in the case-wall Kulite data (Figure 30). This was not consistent with data taken by Payne (Ref. 9) who detected a stall precursor with his hot-film probe. An explanation for this discrepancy could be that the hot-film probe measurements in the present study were contaminated due to probe vibrations.

D. MEASUREMENTS OF 90% SPEED STEAM-INDUCED STALL

Experimental data were acquired through the use of hot-film probes during the steam-induced stall of the compressor at 90% speed. A power spectrum was created using a Fast Fourier Transform in the MATLAB program fft_auto.m (Appendix D). The result gained from the raw data (Figure 33) can be seen in Figure 34. The FFT displayed the strong effect the shock waves propagated upstream from the rotor had on the hot-film, causing geometry effects like once per revolution frequency (406 Hertz) to be blocked, but not the precursor frequency (approximately 250 Hertz).

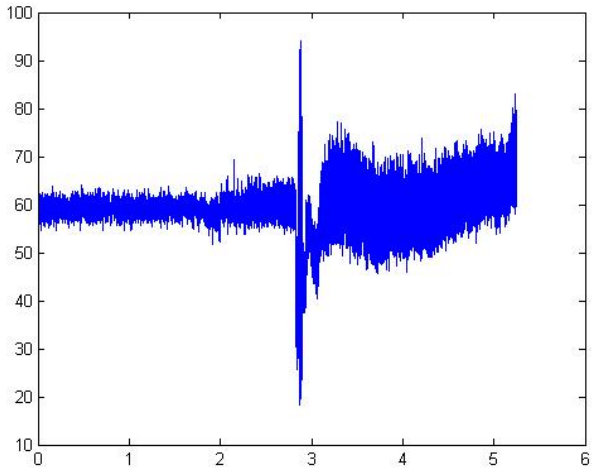

Figure 33. Hot-Film Raw Data at 90% Speed During a Steam-Induced Stall

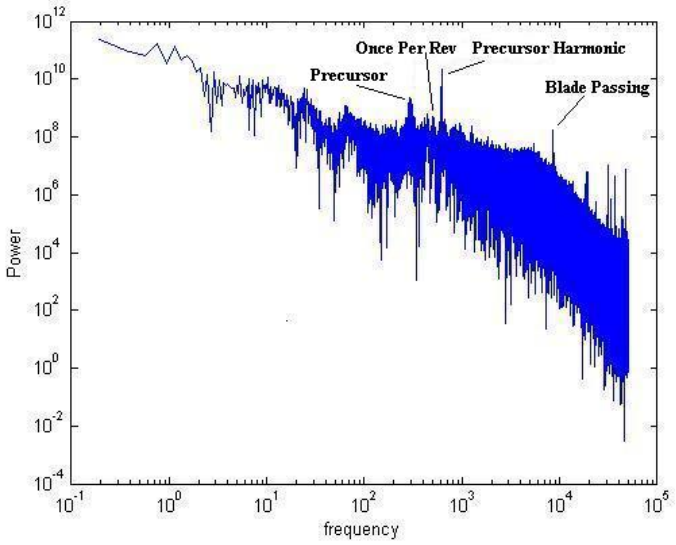

Figure 34. Hot-Film Fast Fourier Transform at 90% Speed During a Steam-Induced Stall

The contour plot of the hot-film, Figure 35, displayed similar effects, making the once per revolution and precursor frequencies difficult to distinguish. The Kulite pressure transducers, placed in the case wall and closer to the rotor, displayed these frequencies with much greater distinction as seen in Figure 36. This plot also reinforced the estimated precursor frequency of 250 Hertz.

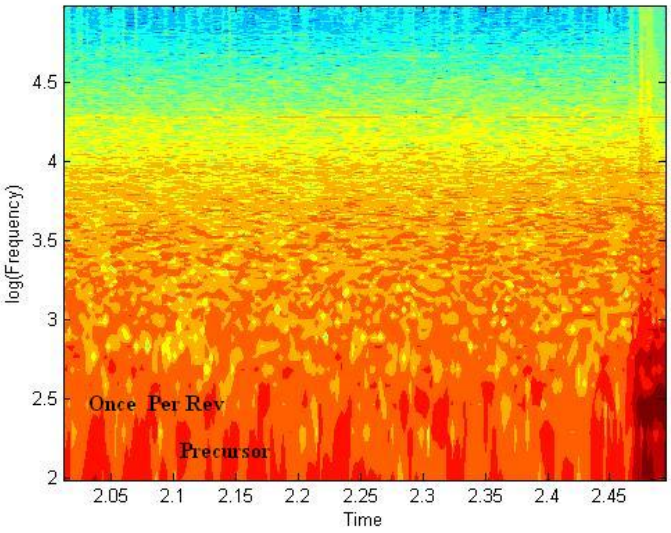

Figure 35. Contour Plot of Hot-Film 1 as Compressor Moves into a 90% Speed Steam-Induced Stall

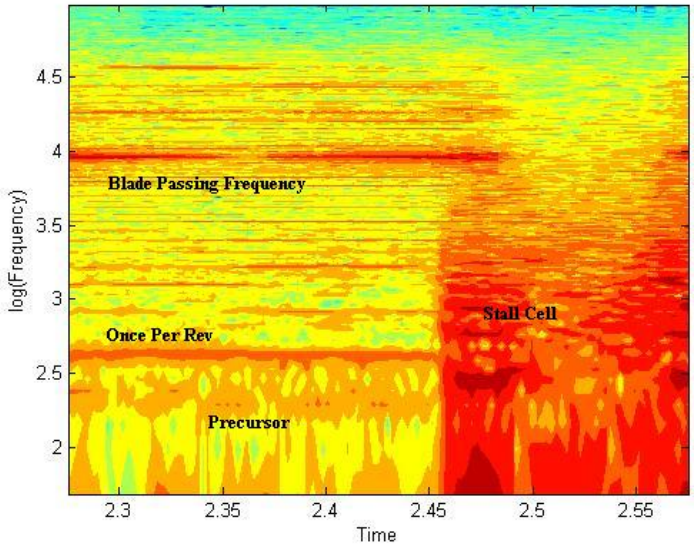

Figure 36. Contour Plot of Kulite 1 as Compressor Moves into a 90% Speed Steam-Induced Stall

E. MEASUREMENTS OF 95% SPEED STEAM-INDUCED STALL

The procedure described in part D was repeated in the TCR for 95% speed steam-induced stall with the results shown in Figures 37 to 40 and additional plots in Appendix F. The precursor frequency (approximately 300 Hertz) and its harmonic dominated the FFT, making the spike expected for the once per revolution frequency (429 Hertz) indiscernible.

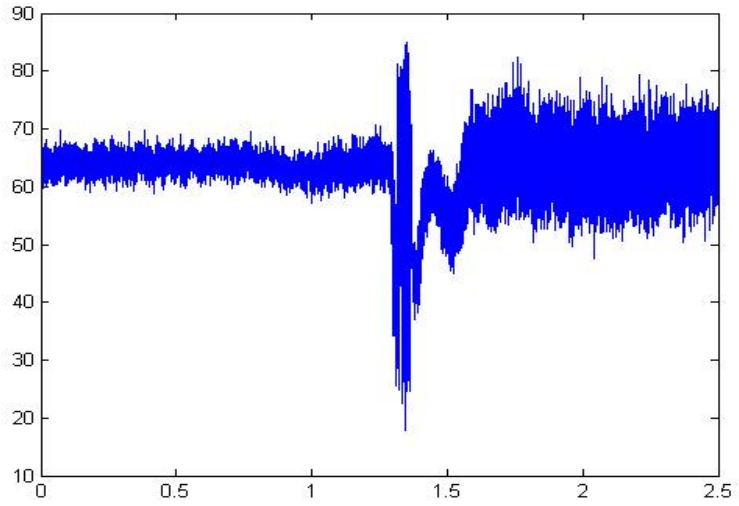

Figure 37. Hot-Film Raw Data at 95% Speed During a Steam-Induced Stall

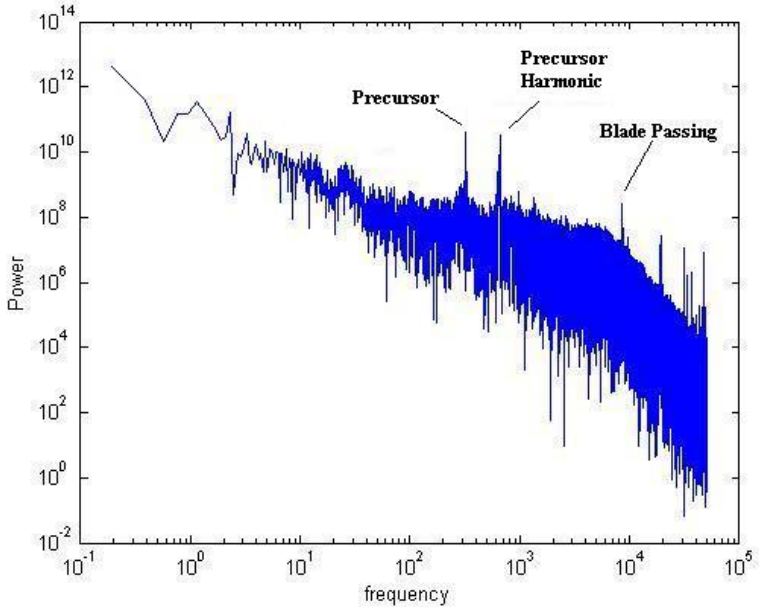

Figure 38. Hot-Film Fast Fourier Transform at 95% Speed During a Steam-Induced Stall

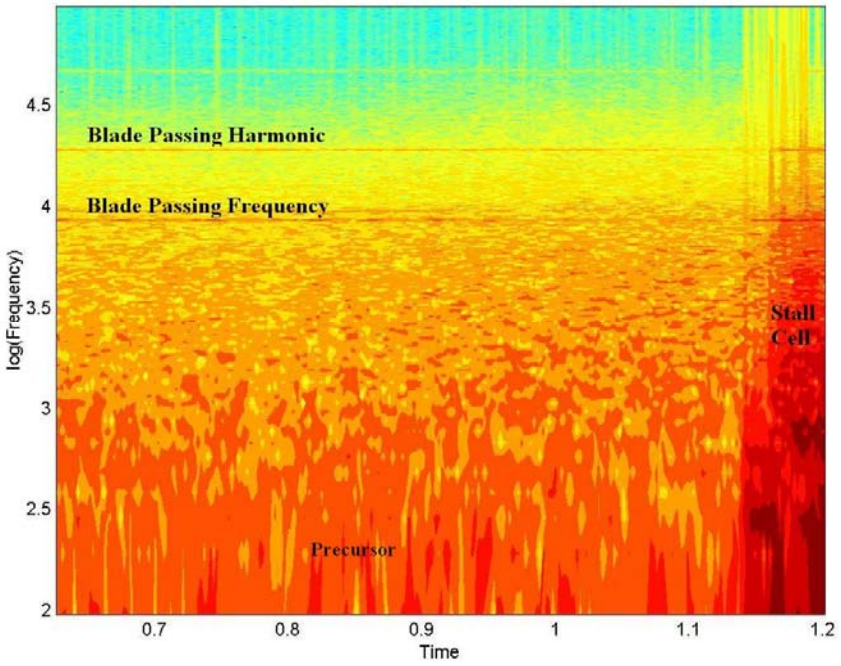

Figure 39. Contour Plot of Hot-Film 1 as Compressor Moves into a 95% Speed Steam-Induced Stall

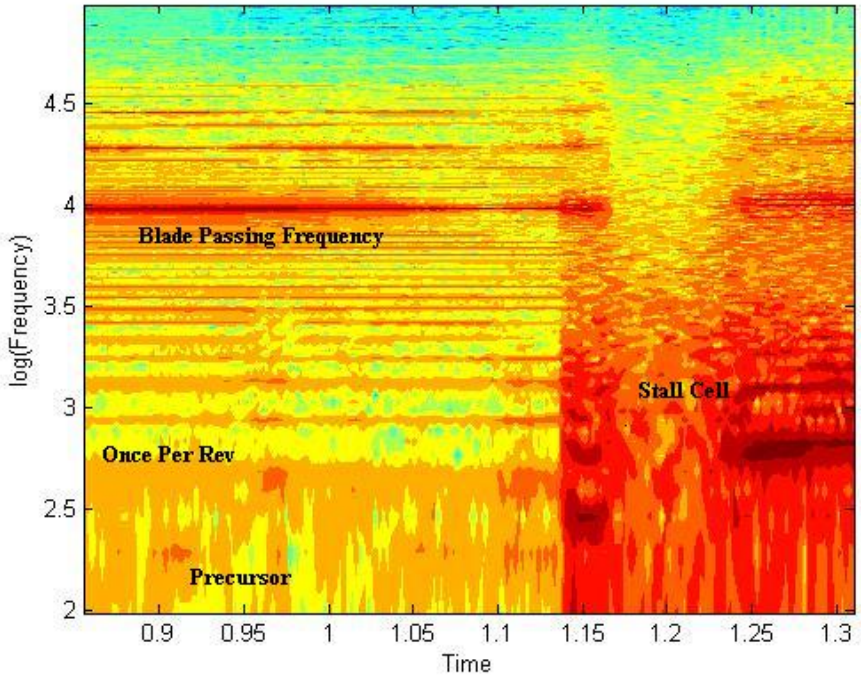

Figure 40. Contour Plot of Kulite 1 as Compressor Moves Into a 95% Speed Steam-Induced Stall

VII. RESULTS AND DISCUSSION OF COMPUTER SIMULATION

A. 90% SPEED SIMULATION

Using the average velocity and k and ε values calculated from experimental data and the CFX-5 computer software, the computer simulated rotor performance was mapped from open throttle to near stall conditions at 90% speed. Figure 41 displays the pressure on the blade and hub and the Mach number distribution at 95% span. Figure 42 is a plot of the static pressure over the surface of the blade at its mid-span at near stall conditions.

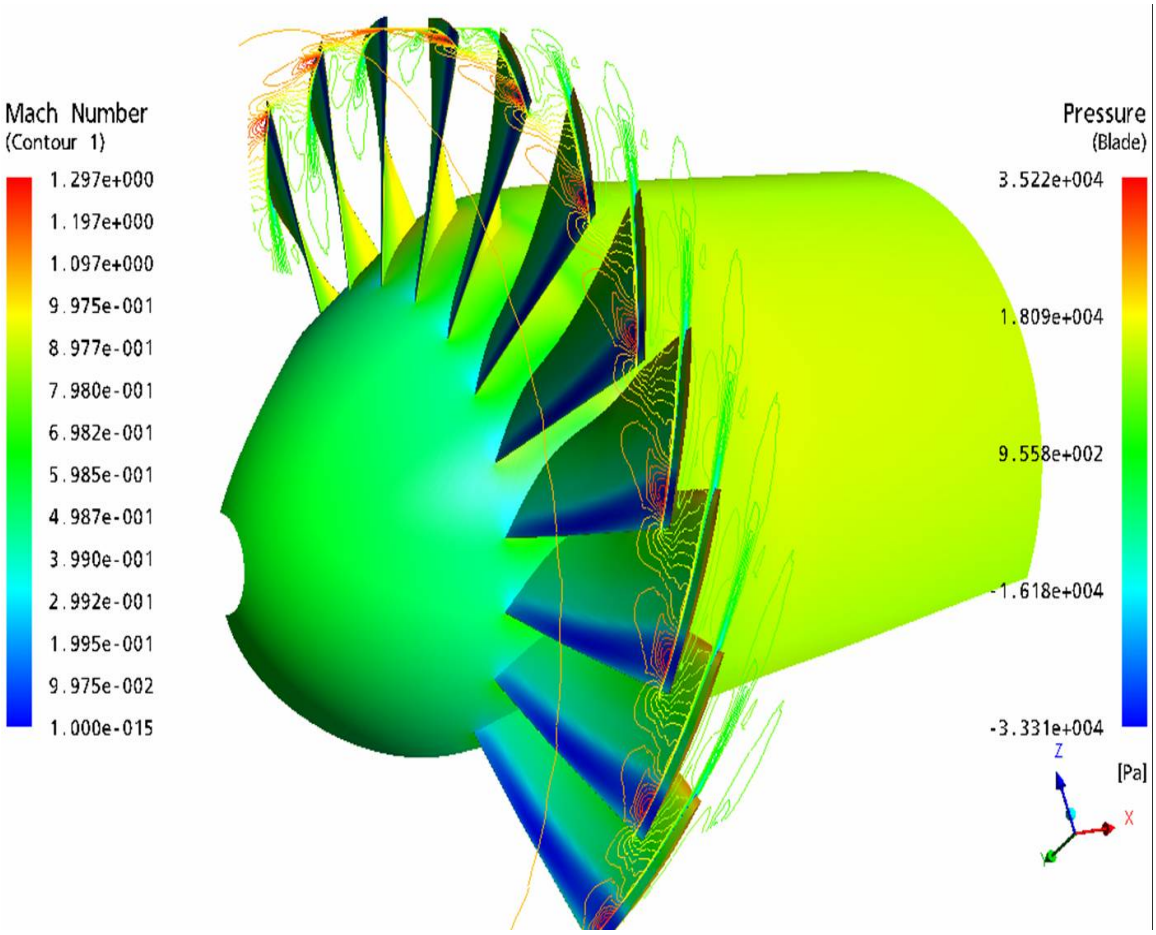

Figure 41. Computer Simulation Model of TCR at 90% Speed Near Stall

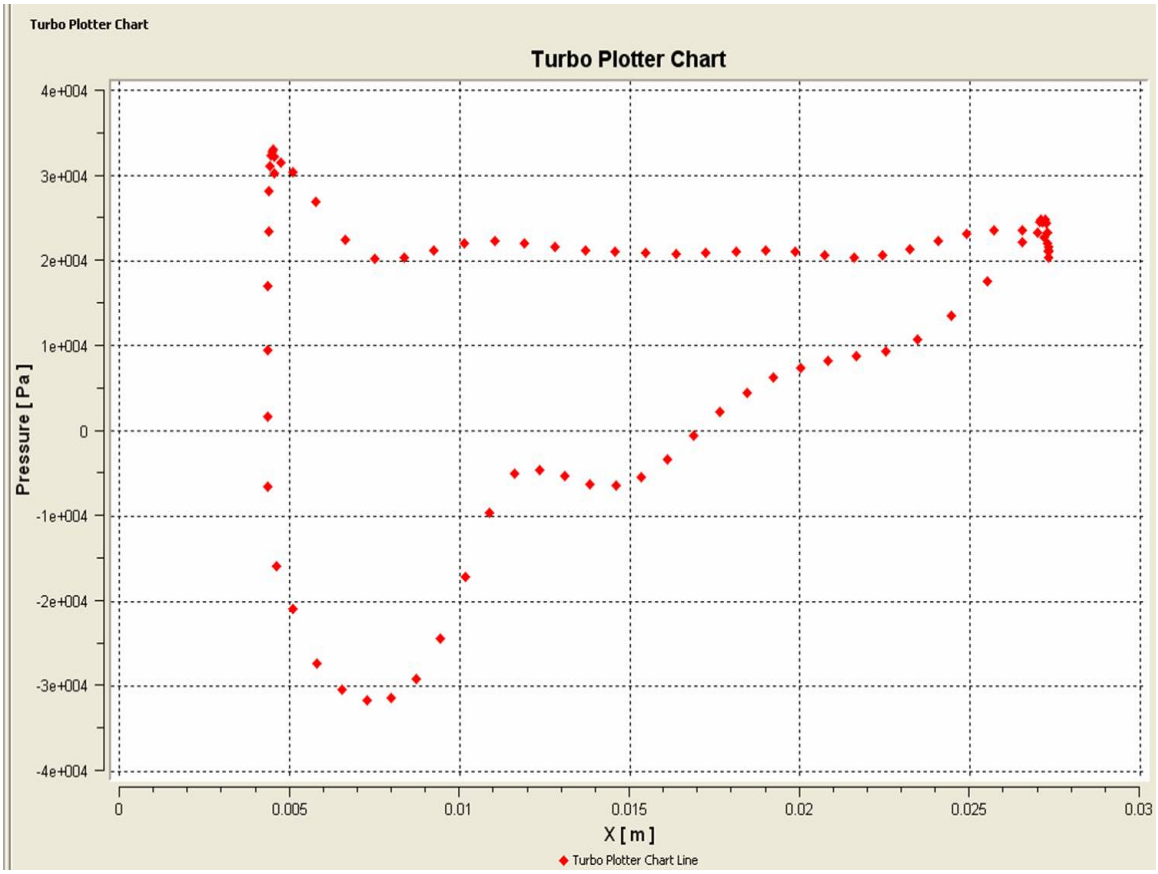

Figure 42. Blade Tip Pressure Distribution at 90% Speed Near Stall

B. 95% SPEED SIMULATION

The process described in part B was repeated for 95% speed. The results are displayed in Figures 43 and 44.

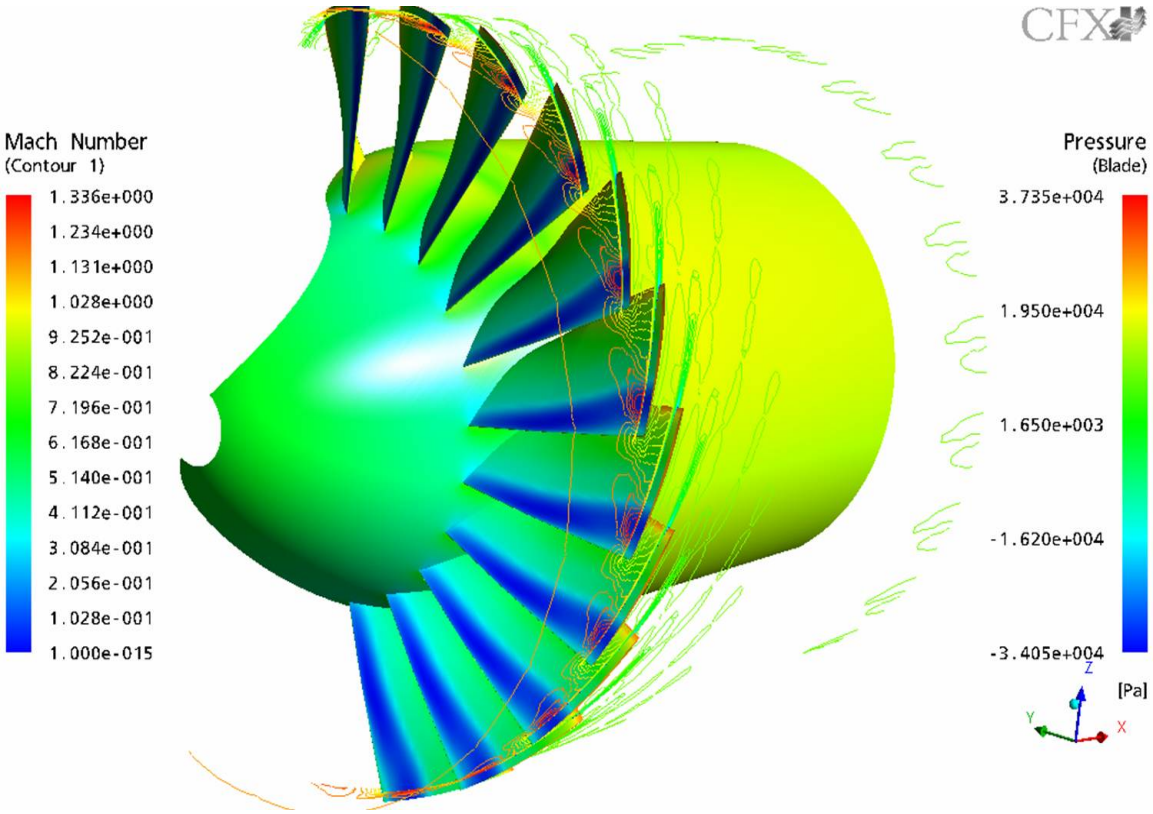

Figure 43. Computer Simulation Model of TCR at 95% Speed Near Stall

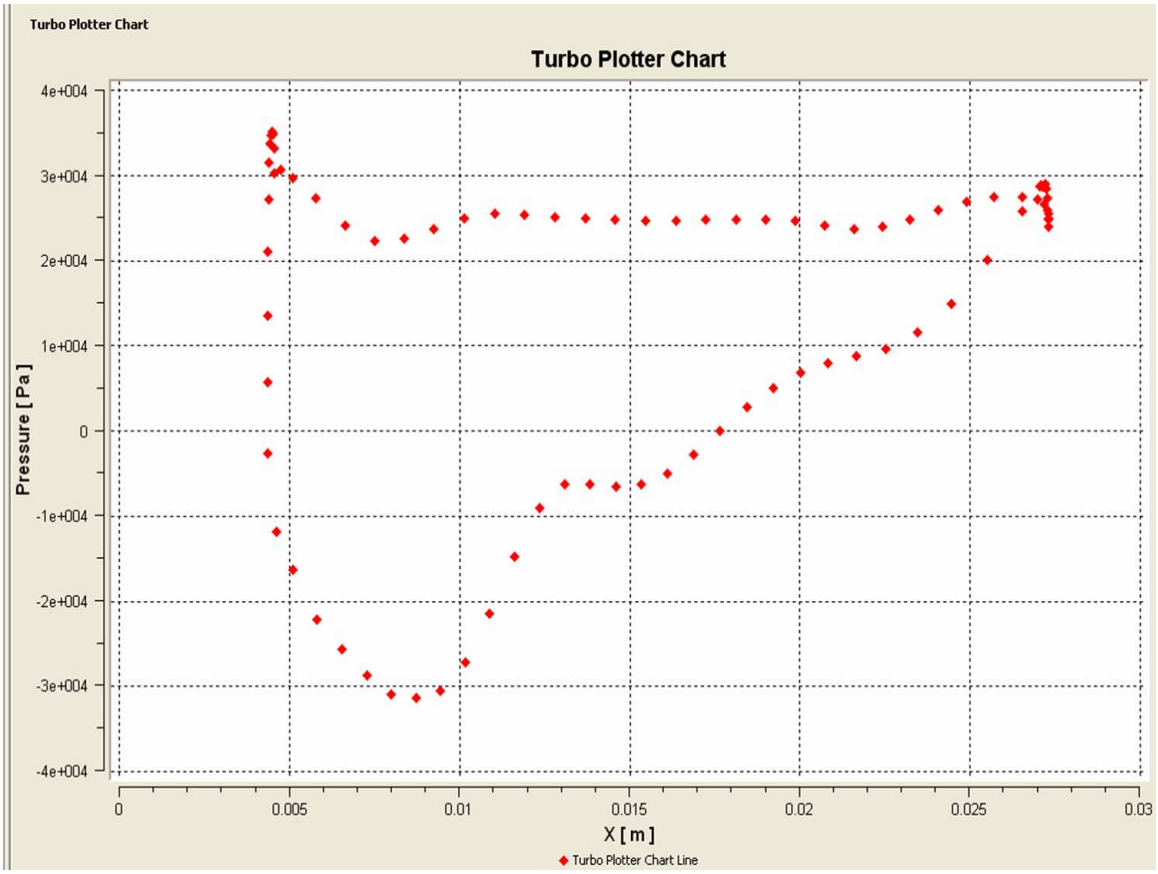

Figure 44. Blade Tip Pressure Distribution at 95% Speed Near Stall

C. COMPARISON OF COMPUTED AND MEASURED PERFORMANCE

The computer simulated values of mass flow rate, total pressure, and total temperature were used to calculate pressure ratio and isentropic efficiency. The spreadsheet results are presented in Appendix G. Figure 45 is a graphical comparison of computer simulated and experimental pressure ratio results. The simulation data follows the general curvature of the experimental data. However, the simulation underestimated the pressure ratio by 2.5 to 4.5% as it approached near stall conditions, and at open throttle, was even less accurate. The simulation also reached stall at a higher mass flow than was found experimentally.

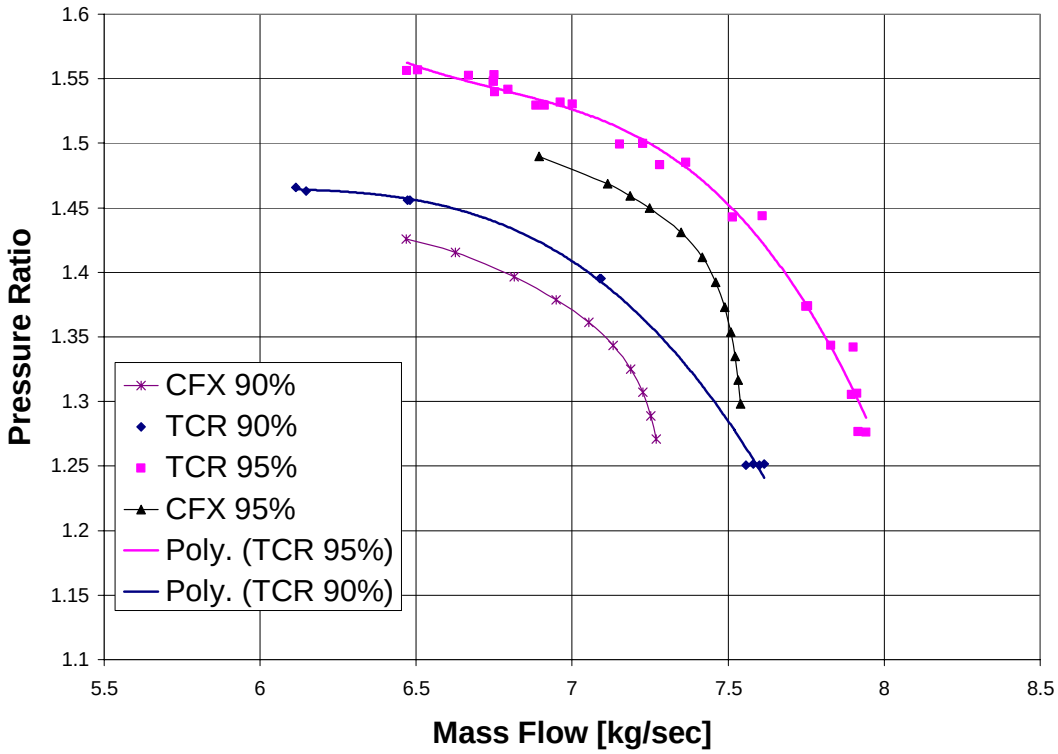

Figure 45. Experimental and Computer Simulated Pressure Ratio vs. Mass Flow for 90 and 95% Speed TCR

Figure 46 shows the experimental and computer simulated efficiency values. As is often the case with current computer models, efficiency was overestimated. In this case, peak efficiency was overestimated by approximately 3.3%, while the mass flow at which the peak occurred was underestimated by approximately 6.5%.

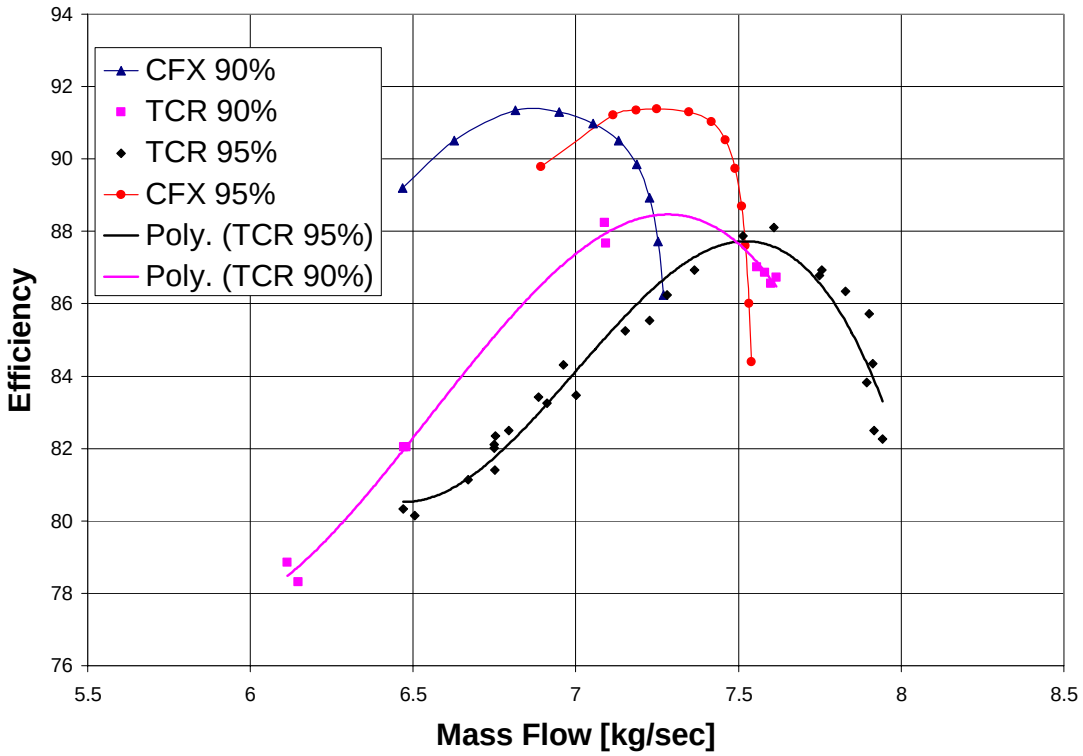

Figure 46. Experimental and Computer Simulated Efficiency vs. Mass Flow for 90 and 95% Speed TCR

VIII. CONCLUSIONS AND RECOMMENDATIONS

A. CONCLUSIONS

1. Compressor Performance

The present experiment provided evidence of the detrimental effect steam ingestion had on the stall line of the compressor. Stall occurred at higher mass flow values when steam was ingested. The presence of steam decreased the density of the fluid flowing through the compressor, causing the compressor to overspeed, then stall. At 90% speed the stall margin was reduced from 0.17 to 0.16 due to steam ingestion and at 95% speed it was reduced from 0.14 to 0.12. Approximately 2% of total mass flow rate of steam was ingested by the rotor for both these speeds. The present investigation was the first transonic tip speed steam-induced stall tests on the TCR.

Although the precursors to stall were as distinctly measured in the present study as those measured previously at 90% and 95% speed, the addition of multiple Kulite probes and back-up hot-film probes proved invaluable in determining stall precursors at transonic rotor tip speeds.

2. Computer Simulation

The CFX-5 software proved to be a relatively accurate modeling system for the transonic compressor. It will prove useful for modeling the effects of steam ingestion in a rotor-only compressor as well as a single or multi-stage compressor at near stall conditions. However the present model is not accurate enough to use for design purposes.

B. RECOMMENDATIONS

The next step is to examine the effects of steam ingestion on a full single stage compressor at near stall conditions. Steam-induced surge could prove catastrophic so care needs to be taken when undertaking such tests.

The computer simulation may be improved by further refining the grid. Modeling of the entire compressor instead of a single blade passage would also provide a more accurate simulation of the compressor. With experimental steam data now available and the CFX-5 software capable of modeling steam as the fluid medium, a model of the compressor during steam ingestion should be attempted.

APPENDIX A. RENAME DSA 3217 IP ADDRESS

Step 1: De-energize DSA. Connect trigger/serial test cable from DSA to I/O port on computer.

Step 2: Create a HyperTerminal
-On computer desktop click START→PROGRAMS→ACCESSORIES →COMMUNICATIONS→HYPERTERMINAL
-Do not make HyperTerminal the default. Click "NO"
-Enter a name and pick symbol
-Connect using COM 1 – or whichever I/O the serial cable is connected to
-Set Parameters → 9600 BAUD, 8 data bits, No parity, 1 stop bit

Step 3: Energize DSA. System information will display.

Step 4: "Press any key to stop auto-boot..." displays. Hit any key within 3 seconds.

Step 5: When the auto-boot process is stopped, type "p" <enter> to get existing parameters.

Step 6: Type "c" <enter> to change parameters. The boot-loader prompts for each parameter. If correct press <enter>.

Step 7: When it gets to "inet on ethernet," type "131.120.20.### (the last 3 numbers will be between 250 and 300).

Step 8: After all changes have been made, verify new settings by typing "p" <enter>.

Step 9: Restart the operating system with the new settings by typing "@" <enter>.

Step 10: If DSA boots correctly, de-energize and disconnect the serial test cable.

THIS PAGE INTENTIONALLY LEFT BLANK

APPENDIX B. HOT-FILM CALIBRATION PROCEDURE

IFA 100 Setup

1. Record current temperature (Ta) and pressure (Pa).
2. Set IFA for appropriate channel [CHANNEL][#][ENTER].
3. Insert shorting probe and measure cable resistance (Rc).
    a. Press [RES MEAS]
    b. Zero with [OPERATE RES] control knob of correct transducer
    c. Press [RES MEAS]
    d. Record Rc then press [ENTER]
4. Replace the shorting probe with the hot wire probe.
5. Repeat step #2 a through c only. DO NOT PRESS ENTER. Record Ro.
6. Press [OPERATE RES] and adjust to hot wire operating resistance (on box cover). Record Rop.
7. Press [BRIDGE COMP] and set with [BRIDGE] control knob according to following table:

Sensor Type	Standard 1
T1.5	35
-P2	83
-PI1.5	115
-PI5	120
Metal Clad	775
-10A	70
-10	70
-20	115
-60	250

8. Press [RUN].
9. Start wind tunnel. Ensure reference pressure is set to 10 inches Hg.

10. Turn [CABLE COMP] knob fully counterclockwise. Turn knob until OSC light comes on then turn clockwise until it goes off plus an extra half turn.

11. Create a new folder for day. Move copy of calibration file 70536123 into folder.

12. On IFA main screen select [CALIBRATION] then [PROBE DATA]

    a. Select [OPEN CAL FILE]

    b. Select file 70536123

    c. Settings as follows:

A/D Chan	Hotwire channel #
IFA Chan	Hotwire channel #
Probe Type	S
Cable	Rc
Opr Res	Rop
Offset	3
Gain	4
Cal Method	Acquire E & Type dP Manual

13. Select [CALIBRATE].

14. Enter current conditions on the left hand side of the screen remembering to select appropriate dP unit. The dP is the difference between static and stagnation pressure (Ports 6 + 48) and is used by the software to calculate the average velocity for each calibration point.

15. On the right side of the screen, enter the number of calibration points to be taken (usually 8).

16. For each calibration point, enter dP and the press enter or click mouse outside of dP box. The IFA software should have calculated a velocity from the dP reading. Press [Acquire] to record calibration point. Record data on calibration sheet.

17. After all calibration points have been taken, close graph and press [Next Screen].

18. Select [Curves].

19. At bottom of screen, in the “fit” block, select King’s Law. Record King’s Law coefficients on calibration sheet.

20. Open new calibration file in Notepad. Change probe number on lines 2 and 6 to appropriate number and save.

THIS PAGE INTENTIONALLY LEFT BLANK

APPENDIX C. HOT-FILM MEASUREMENTS

1. Create new folder with today's date.
2. Copy probe calibration files into new folder.
3. On main menu, select "Acquisition" then "Probe Table."
4. In Experiment box, select "Get File." Open newly created folder. Name new file, e.g. 90_PE.R0001 for 90% speed peak efficiency.
5. Click on "Add Probe."
6. Select calibration file for channel 1 transducer.
7. Repeat steps 5 and 6 for channel 2.
8. Ensure both channels have asterisks. If not, select channel and press "Tag A/D."
9. Click "Next Screen."
10. Update "Atm Pressure" and various units.
11. Set sample rate to 100,000 Hertz, size to 8 kpts/ch.
12. Click "Next Screen."
13. Once TCR speed steady, click "Trigger" to record data.

THIS PAGE INTENTIONALLY LEFT BLANK

APPENDIX D. MATLAB CODE

A. HW.M

```
%   This script will calculate the average velocity and
%   turbulence intensity of up to four probes by first
%   sending raw data into matrix "a" and then expanding
%   the matrix with the calculated instantaneous velocities.
%   The velocities from probes 1,2,3,4 will be placed in
%   in columns 6,7,8,9 respectively, irregardless of the number
%   of probes used.

%file=input('Enter probe data file with single quotes in this format: filename.Exxx')

% format for file is '13JUL05.E0005'

% kings law coeff must be in a matrix with probes as rows. (a b n)
% for example k=[.87726 .31691 .5]

king=[-23.44088 20.06122 0.11];

a=dlmread('90_OPEN.E0003');

   for n=1:length(a)
      a(n,2);
      expo=1/king(1,3);
      E2=a(n,2)*a(n,2);
      a(n,3)=((E2-king(1,1))/(king(1,2)))^expo;
```

```
end

%   Calculate the mean velocity

avevel_1=mean(a(:,3))
sd_1=std(a(:,3));

%   And the turbulence intensity from the standard deviation

turbint_1=(sd_1*100)/avevel_1

%   FFT
time=a(:,1);
lengtht=length(time);
deltat=(time(lengtht,1)-a(1,1))/lengtht
plot(time,a(:,3))
Y=fft(a(:,3));
Y(1)=[];
nn=length(Y);
power=abs(Y(1:nn/2)).^2;
nyquist=1/2;
%   freq=(1:nn/2)/(nn/2)*nyquist;
freq = (1:nn/2)/(nn*deltat);
figure
loglog(freq,power)
xlabel('frequency')
ylabel('Power')
```

B. FFT_AUTO.M

```
%   Script to plot the FFT and Autocorrelation of a hotwire signal


close all

clear all


a=dlmread('90_PE.E0005');

%time=a(1:1024,1);

%voltage=a(1:1024,2);


time=a(:,1);

voltage=a(:,2);


figure(1)

plot(time,voltage)

xlabel('time')

ylabel('voltage')

title('Raw Signal')


N=length(voltage)-1;

deltat=.00001;


Y = fft(voltage);

Y(1)=[];

n=length(Y);

power = abs(Y(1:n/2)).^2;

nyquist = .5;
```

```
%freq = (1:n/2)/(n/2)*nyquist;
freq = (1:N/2)/(N*deltat);
figure(2)
loglog(freq,power)
%semilogy(freq,power)
xlabel('freq')
ylabel('power')
title('Periodogram')

figure(3)
ave_volt=mean(voltage);
volt=voltage-ave_volt;
%Plot the fluctuating voltage
plot(time,volt)
figure(4)
%No. of points to take the autocorrelation over
m=8192;
[C,lags]=xcorr(volt,m,'coeff');
%plot(time,C)

plot(lags,C)

figure(5)
auto_time=deltat*lags;
plot(auto_time,C)
grid on
```

APPENDIX E. 95% SPEED PEAK EFFICIENCY AND NEAR STALL AUTOCORRELATION AND CONTOUR PLOTS

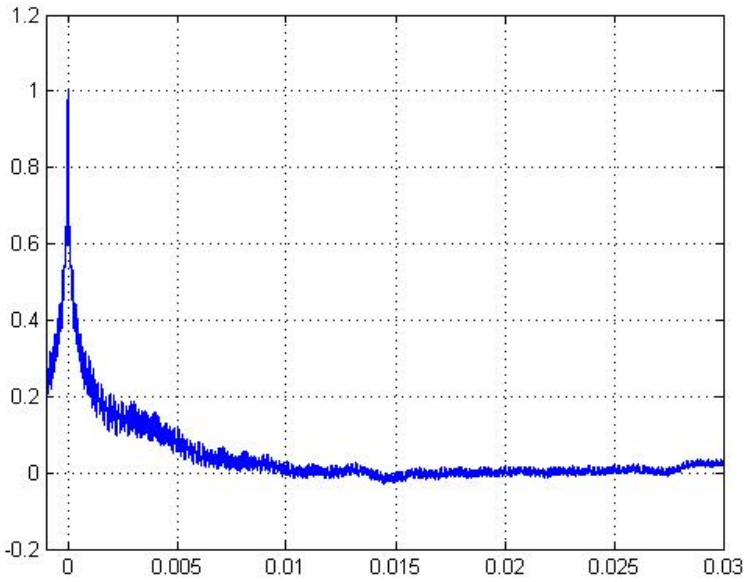

Figure 47. Auto-Correlation of Hot-Film Data at 90% Speed Near Stall

$\Delta t \approx 0.002$ (From above graph)

$Ti = 0.019$ (Turbulence intensity from hw1.m)

$U_{avg} = 65.8$ (Average velocity from hw1.m)

$u'^2 = (Ti * U_{avg})^2 = 1.563$

$k = 1.5*(u'^2) = 2.3445$

$L = \Delta t * U_{avg} = 0.1316$ (Turbulence length)

$\varepsilon = (C^{0.75} * k^{1.5})/(\kappa * L) = 11.206$ ($C = 0.09$, $\kappa = 0.4$)

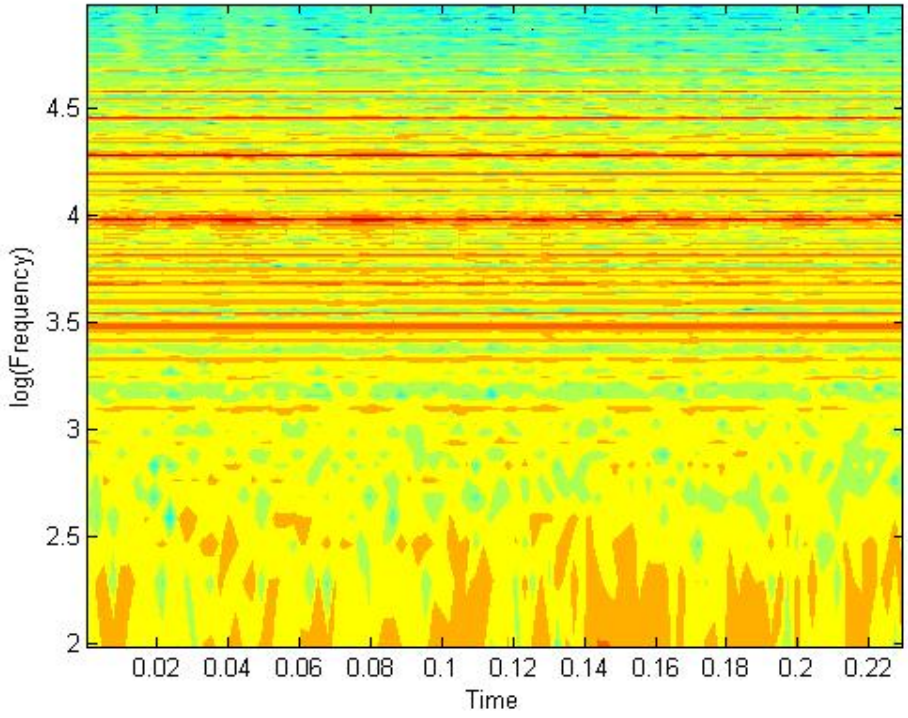

Figure 48. Kulite 1 at 95% Speed Peak Efficiency

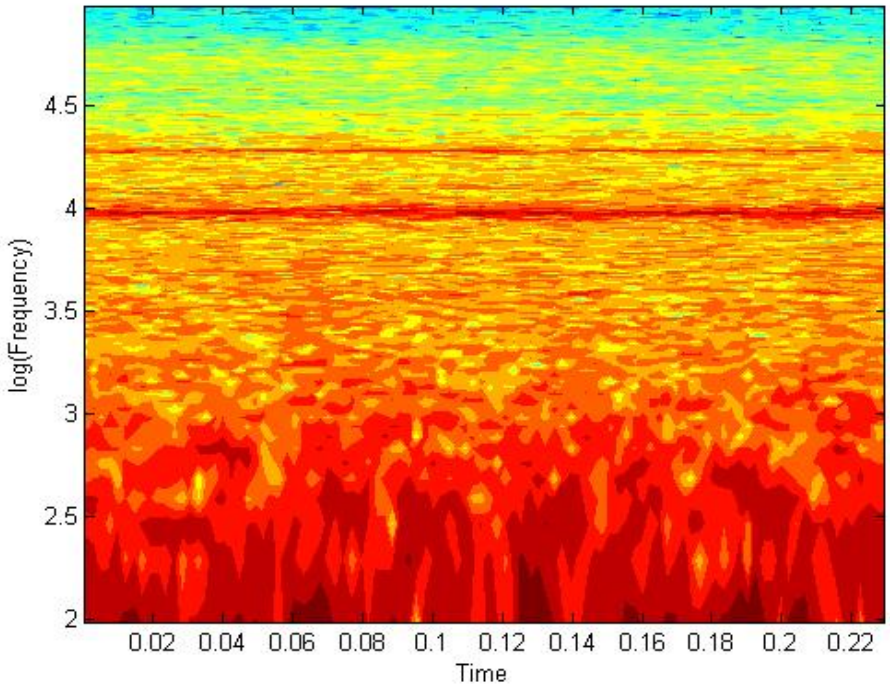

Figure 49. Impact Probe at 95% Speed Peak Efficiency

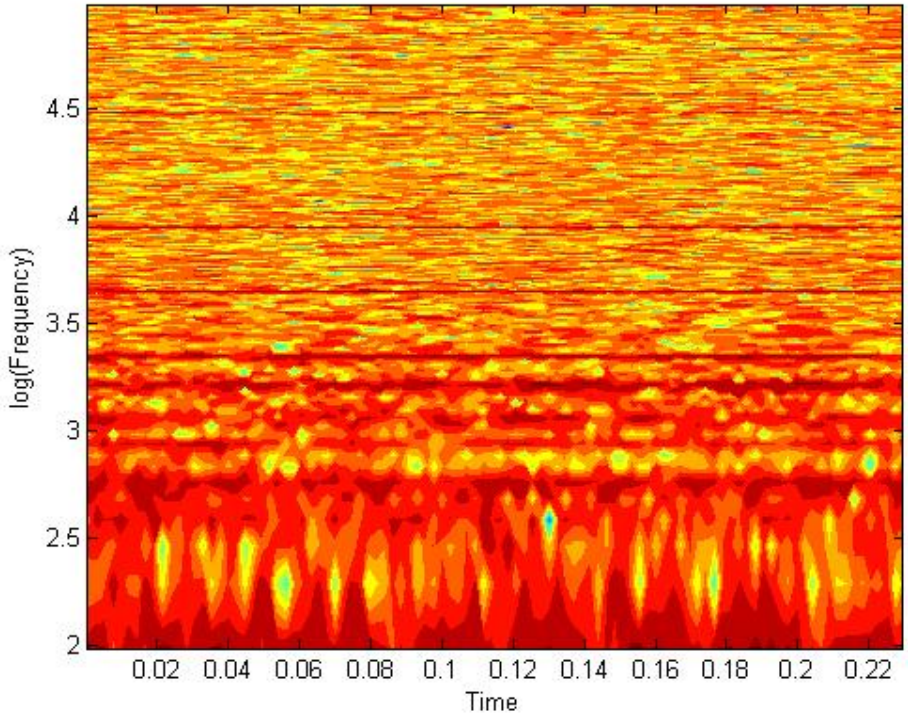

Figure 50. Hot-Film 1 at 95% Speed Peak Efficiency

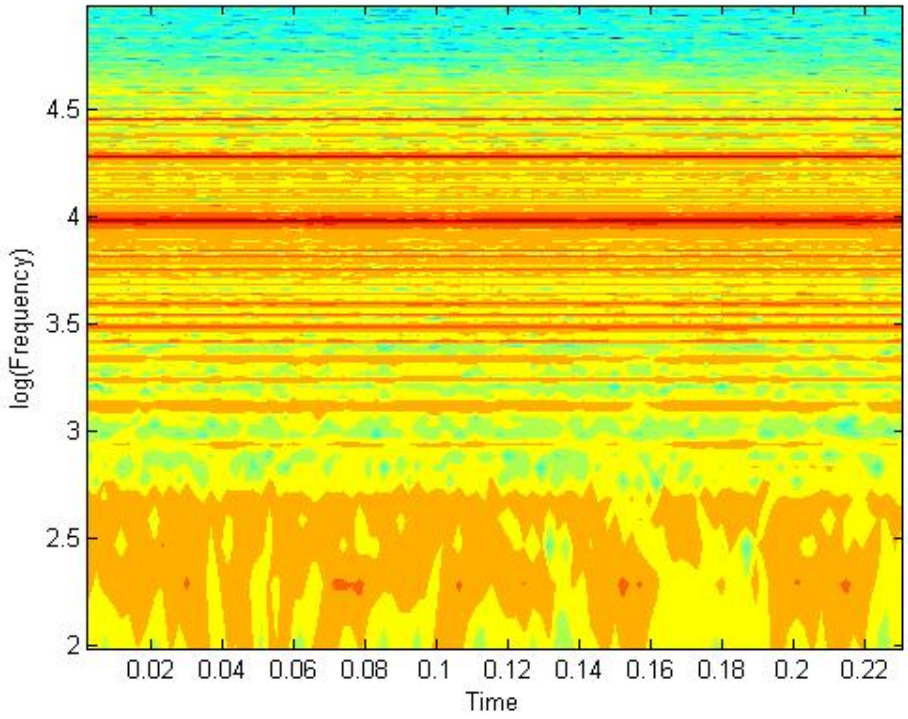

Figure 51. Kulite 1 at 95% Speed Near Stall

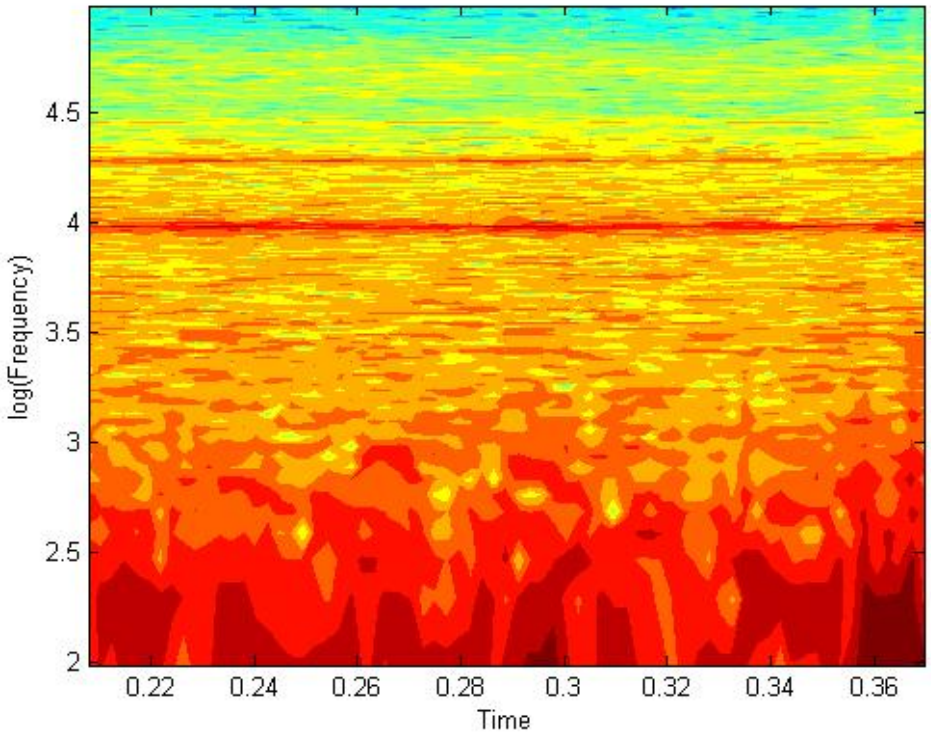

Figure 52. Impact Probe at 95% Speed Near Stall

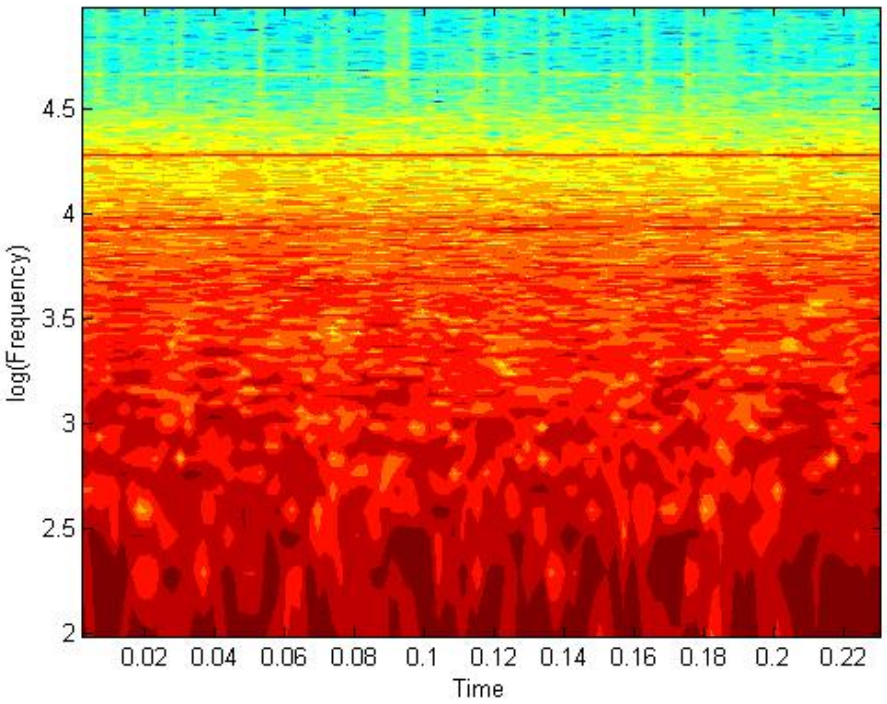

Figure 53. Hotfilm 1 at 95% Speed Near Stall

APPENDIX F. KULITE CONTOUR PLOTS FOR 90% AND 95% SPEED: STEAM INDUCED STALL

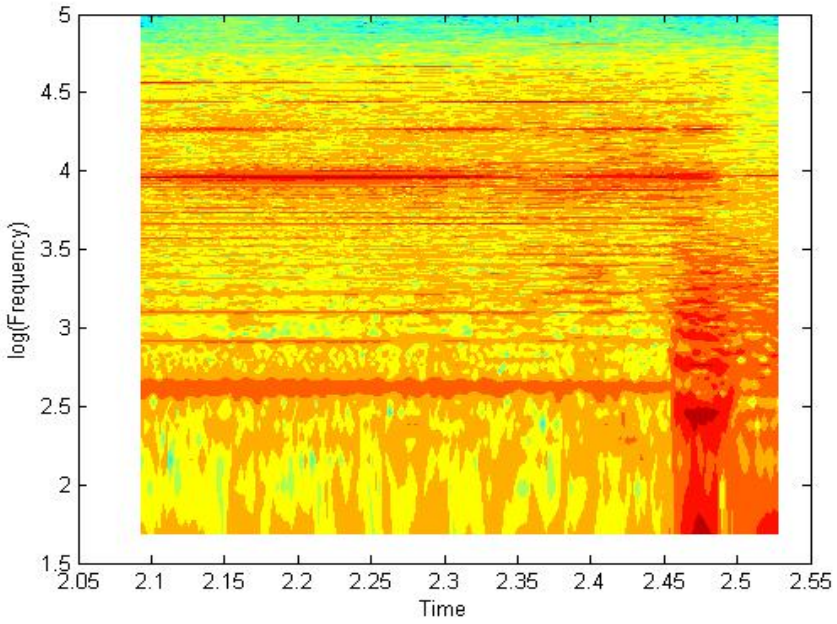

Figure 54. Kulite 2 at 90% Speed Steam-Induced Stall

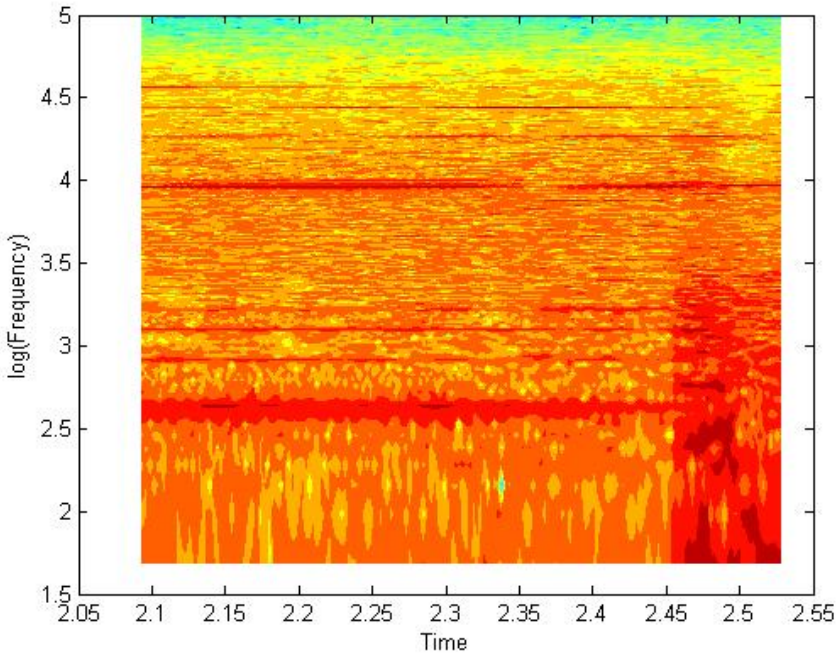

Figure 55. Kulite 3 at 90% Speed Steam-Induced Stall

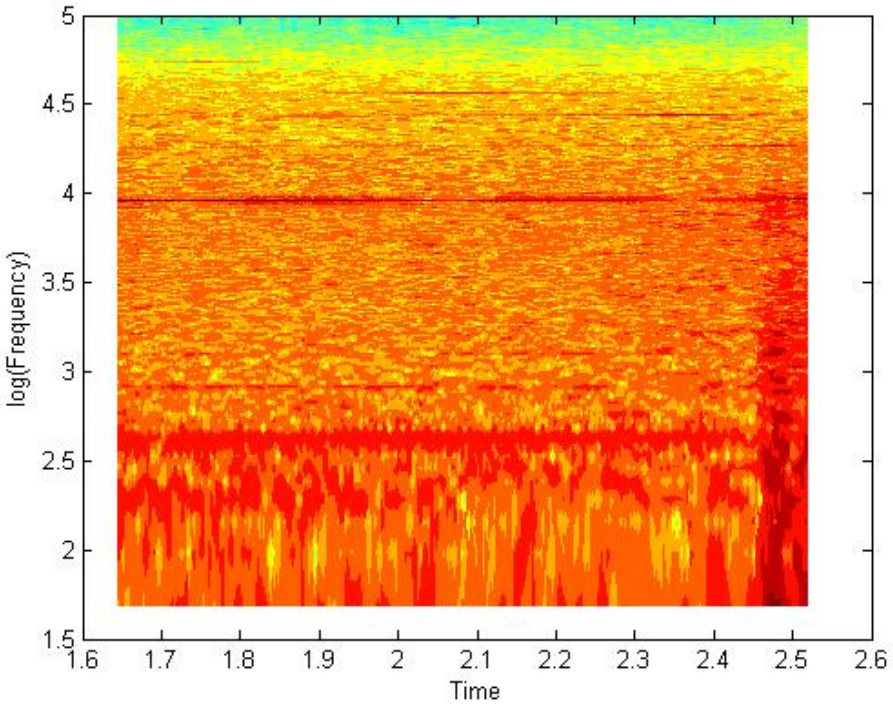

Figure 56. Kulite 4 at 90% Speed Steam-Induced Stall

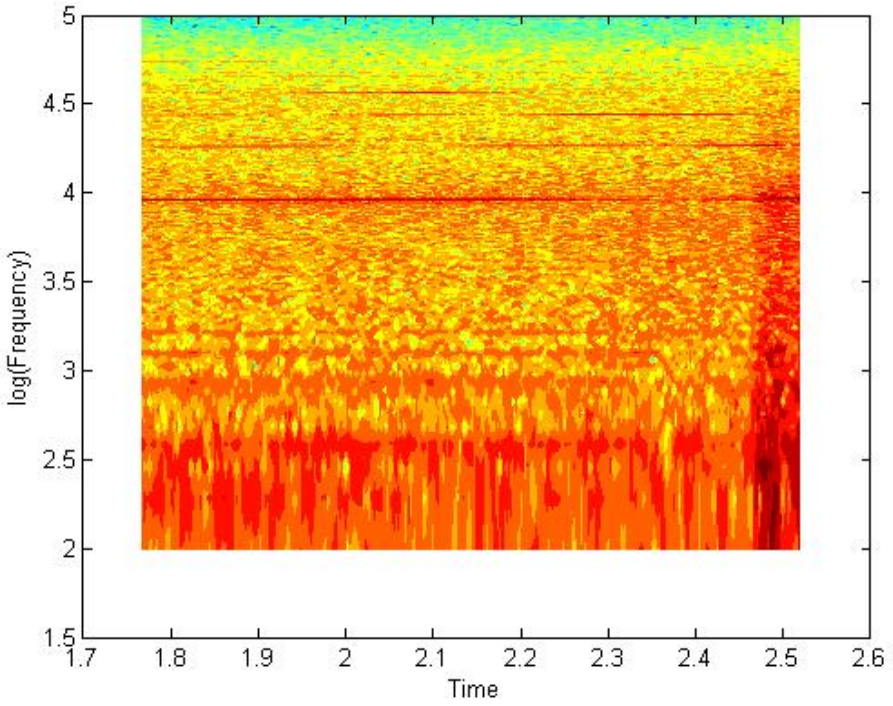

Figure 57. Kulite 5 at 90% Speed Steam-Induced Stall

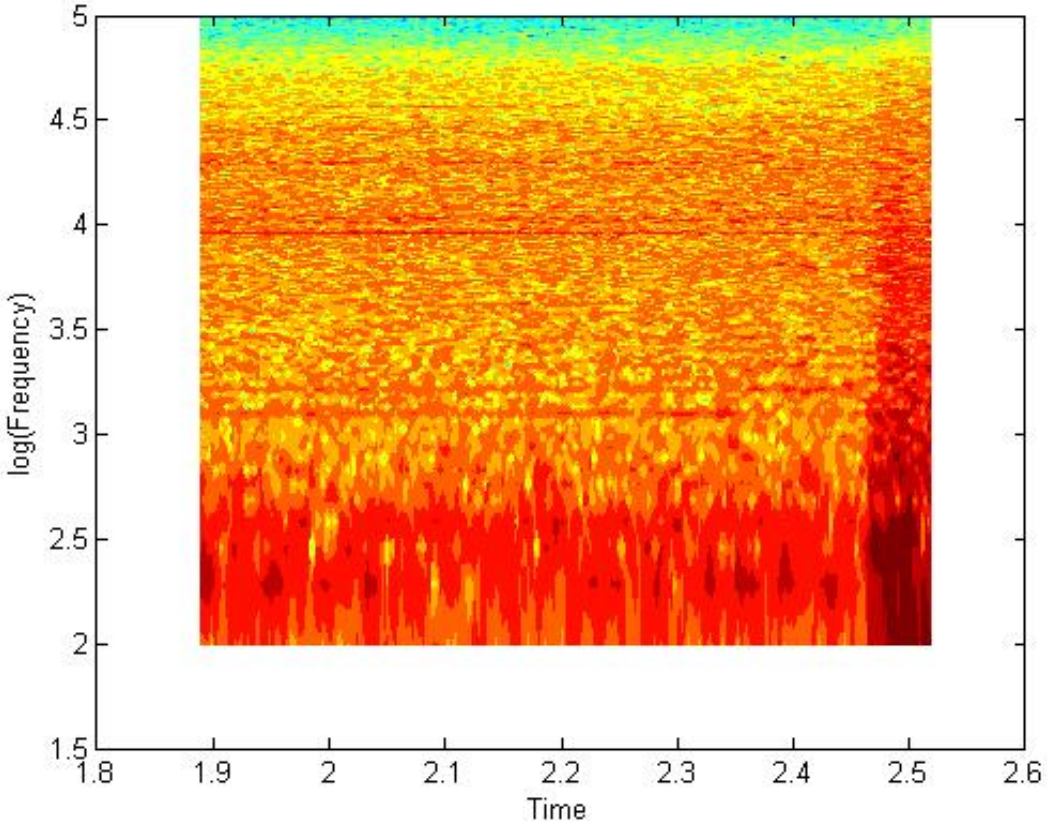

Figure 58. Kulite 6 at 90% Steam-Induced Stall

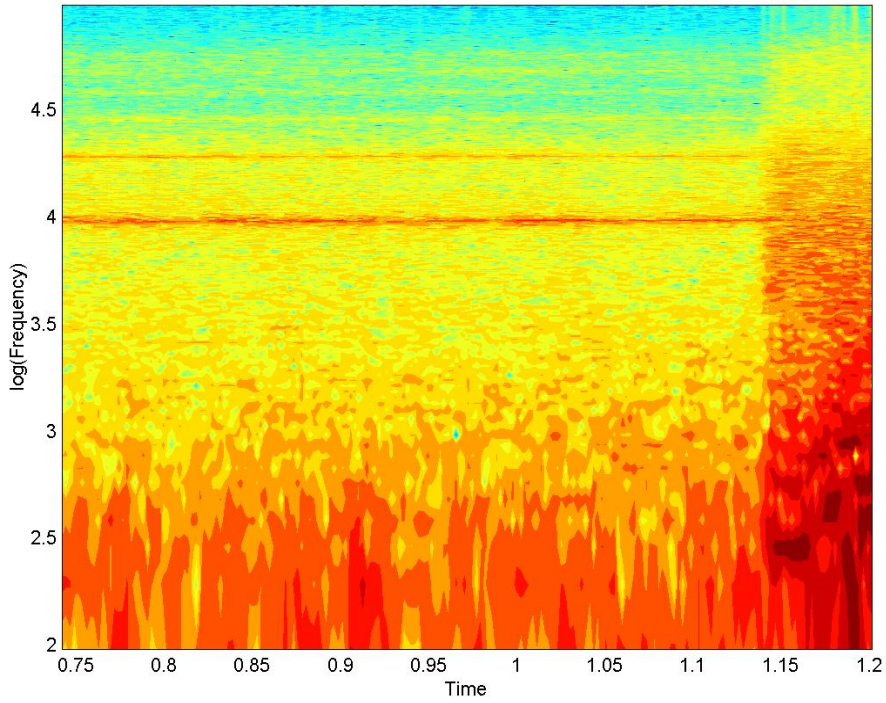

Figure 59. Impact Kulite at 95% Speed Steam-Induced Stall

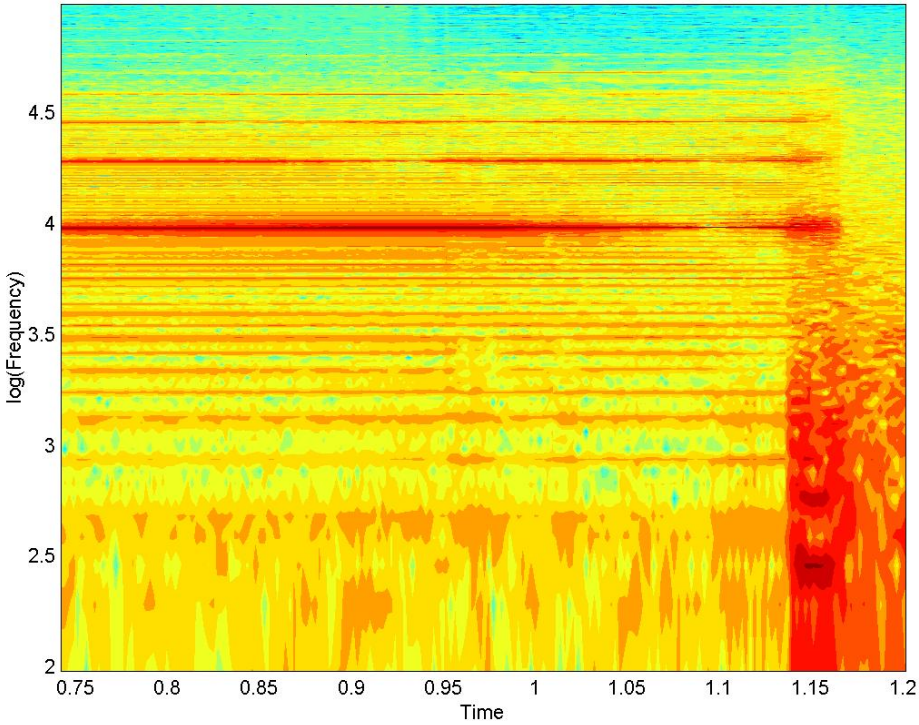

Figure 60. Kulite 1 at 95% Speed Steam-Induced Stall

APPENDIX G. CFX RESULTS

CFX at 90%								
Run #	**mdot ave**	**Pt in abs**	**Pt out abs**	**Pi**	**T in**	**Tout**	**Tao**	**Efficiency**
TCR_0	7.2700	101329	128781	1.2709	300.0	324.6	1.0822	86.24
TCR_2	7.2518	101329	130598	1.2888	299.9	325.6	1.0857	87.72
TCR_4	7.2259	101329	132433	1.3070	299.9	326.7	1.0894	88.93
TCR_6	7.1876	101329	134278	1.3252	299.8	327.7	1.0932	89.85
TCR_8	7.1318	101329	136118	1.3433	299.7	328.8	1.0972	90.51
TCR_10	7.0529	101329	137926	1.3612	299.5	329.8	1.1012	90.98
TCR_12	6.9486	101329	139714	1.3788	299.3	330.8	1.1053	91.29
TCR_14	6.8140	101329	141520	1.3966	299.0	331.8	1.1096	91.35
TCR_16	6.6255	101329	143403	1.4152	298.6	333.1	1.1153	90.51
TCR_17	6.4686	101329	144474	1.4258	298.3	334.0	1.1196	89.19
TCR_18	3.7401	101313	136621	1.3485	295.4	330.3	1.1179	75.62
CFX at 95%								
Run #	**mdot ave**	**Pt in abs**	**Pt out abs**	**Pi**	**T in**	**Tout**	**Tao**	**Efficiency**
TCR_0	7.5392	101329	131541	1.2981	300.6	328.1	1.0917	84.39
TCR_2	7.5324	101329	133391	1.3164	300.6	329.1	1.0950	86.01
TCR_4	7.5220	101329	135251	1.3348	300.5	330.0	1.0982	87.61
TCR_6	7.5093	101329	137189	1.3539	300.5	331.1	1.1020	88.69
TCR_8	7.4895	101329	139124	1.3730	300.5	332.2	1.1056	89.73
TCR_10	7.4604	101329	141084	1.3923	300.4	333.3	1.1096	90.52
TCR_12	7.4166	101329	143064	1.4119	300.3	334.5	1.1138	91.02
TCR_14	7.3481	101329	145019	1.4312	300.1	335.6	1.1181	91.29
TCR_16	7.2485	101329	146922	1.4499	299.9	336.7	1.1225	91.39
TCR_17	7.1863	101329	147872	1.4593	299.8	337.2	1.1248	91.35
TCR_18	7.1141	101329	148838	1.4689	299.6	337.8	1.1273	91.20
TCR_20	6.8936	101329	150955	1.4897	299.1	339.3	1.1344	89.78
TCR_22	3.3971	100634	140799	1.3991	294.7	336.8	1.1429	70.48

THIS PAGE INTENTIONALLY LEFT BLANK

LIST OF REFERENCES

1. Sanger, N.L. "Design of a Low Aspect Ratio Transonic Compressor Stage Using CFD Techniques," ASME Journal of Turbomachinery, Vol. 118, pp. 479-491, July 1996.

2. Sanger, N. L., "Design Methodology for the NPS Transonic Compressor," TPL Technical Note 99-01, August 1999.

3. Gannon, A.J., Hobson, G.V. and Shreeve, R.P., "A Transonic Compressor Stage Part 1: Experimental Results, "ASME GT2004-53923, Turbo Expo, Vienna Austria, June 14-17, 2004.

4. Gannon, A.J., Hobson, G.V. and Shreeve, R.P., "Measurement of the Unsteady Casewall Pressures Over a Rotor of a Transonic Fan and Comparison with Numerical Predictions," ISABE 2005, 17th International Symposium on Airbreathing Engines, Munich, September 2005.

5. Gannon, A.J., Hobson, G.V., Shreeve, R.P., and Villescas, I.J., "Experimental Investigation during Stall and Surge in a Transonic Fan Stage & Rotor-Only Configuration," ASME GT2006-90925, Turbo Expo, Barcelona, Spain, May 8-11, 2006.

6. Rodgers, M. W. Unsteady Pressure Measurements on the Case Wall of a Transonic Compressor, Master's Thesis, Naval Postgraduate School, Monterey, California, June 2003.

7. Villescas, I., Flow Field Surveys In a Transonic Compressor Prior To Inlet Steam Ingestion Tests, Master's Thesis, Naval Postgraduate School, Monterey, California, September 2005.

8. Brunner, M.D., Experimental and Computational Investigation of Flow in a Transonic Compressor Inlet, Master's Thesis, Naval Postgraduate School, Monterey, California, September 2005.

9. Payne, T. A., Inlet Flow-Field Measurement of a Transonic Compressor Rotor Prior to and During Steam-Induced Rotating Stall, Master's Thesis, Naval Postgraduate School, Monterey California, December 2005.

10. Levis, W. R., Unsteady Casewall Pressure Measurements in a Transonic Compressor During Steam Induced Stall, Master's Thesis, Naval Postgraduate School, Monterey California, December 2005.

11. Bochette, N. J., Computational Analysis of Flow Through a Transonic Compressor Rotor, Master's Thesis, Naval Postgraduate School, Monterey California, September 2005.

12. Sussman Automatic Corporation. "SVS6 Electric Steam Boiler Specifications," 2004, Long Island City, New York.

13. Scanivalve Corp. Digital Sensor Array Instruction and Service Manual, January 2005.

14. HP VEE Pro (Version 6.01), August 2000.

15. Yu, H., Private Communication, ICEM-CFD Geometry of a Single Blade Passage, April 2006.

16. MATLAB (version 5.3.0 R11), January 1999.

INITIAL DISTRIBUTION LIST

1. Defense Technical Information Center
   Ft. Belvoir, Virginia

2. Dudley Knox Library
   Naval Postgraduate School
   Monterey, California

3. Distinguished Professor and Chairman Anthony Healey
   Department of Mechanical and Aeronautical Engineering
   Naval Postgraduate School
   Monterey, California

4. Professor Raymond Shreeve
   Department of Mechanical and Aeronautical Engineering
   Naval Postgraduate School
   Monterey, California

5. Professor Garth Hobson
   Department of Mechanical and Aeronautical Engineering
   Naval Postgraduate School
   Monterey, California

6. Dr. Anthony Gannon
   Department of Mechanical and Aeronautical Engineering
   Naval Postgraduate School
   Monterey, California

7. Naval Air Warfare Center
   Propulsion and Power Engineering
   ATTN: Mark Klien
   Patuxent River, Maryland

8. LT Sarah Zarro
   Monterey, California